UNIVERSITY OF ALBERTA

PERFORMANCE OF ADAPTIVE ANTENNA ARRAY ALGORITHMS ON THE IS-95 REVERSE LINK

By

William King Kwong Kong ©

A thesis submitted to the Faculty of Graduate Studies and Research in partial fulfillment of the requirement for the degree of Master of Science.

DEPARTMENT OF ELECTRICAL ENGINEERING

Edmonton, Alberta

Fall 1997

National Library of Canada
Acquisitions and Bibliographic Services
395 Wellington Street
Ottawa ON K1A 0N4
Canada

Bibliothèque nationale du Canada
Acquisitions et services bibliographiques
395, rue Wellington
Ottawa ON K1A 0N4
Canada

Your file Votre référence

Our file Notre référence

The author has granted a non-exclusive licence allowing the National Library of Canada to reproduce, loan, distribute or sell copies of this thesis in microform, paper or electronic formats.

L'auteur a accordé une licence non exclusive permettant à la Bibliothèque nationale du Canada de reproduire, prêter, distribuer ou vendre des copies de cette thèse sous la forme de microfiche/film, de reproduction sur papier ou sur format électronique.

The author retains ownership of the copyright in this thesis. Neither the thesis nor substantial extracts from it may be printed or otherwise reproduced without the author's permission.

L'auteur conserve la propriété du droit d'auteur qui protège cette thèse. Ni la thèse ni des extraits substantiels de celle-ci ne doivent être imprimés ou autrement reproduits sans son autorisation.

0-612-22617-4

Canada

UNIVERSITY OF ALBERTA

RELEASE FORM

NAME OF AUTHOR: **William King Kwong Kong**

TITLE OF THESIS: **Performance of Adaptive Antenna Array Algorithms on the IS-95 Reverse Link**

DEGREE: **Master of Science**

YEAR THIS THESIS GRANTED: **1997**

Permission is hereby granted to the University of Alberta Library to reproduce single copies of this thesis and to lend or sell such copies for private, scholarly, or scientific research purposes only.

The author reserves all other publication and other rights in association with the copyright in the thesis, and except as hereinbefore provided, neither the thesis nor any substantial portion thereof may be printed or otherwise reproduced in any material form whatever without the author's prior written permission.

Kong King Kwong

#1102, 8515-112st,
Newton Place,
Edmonton, A.B., Canada.
T6G 1K7

Date : Oct. 3, 97

UNIVERSITY OF ALBERTA

FACULTY OF GRADUATE STUDIES AND RESEARCH

The undersigned certify that they have read, and recommend to the Faculty of Graduate Studies and Research for acceptance, a thesis entitled **PERFORMANCE OF ADAPTIVE ANTENNA ARRAY ALGORITHMS ON THE IS-95 REVERSE LINK** submitted by **William King Kwong Kong** in partial fulfillment of the requirements for the degree of **Master of Science**.

W. Krzymien

Dr. Witold A. Krzymien, Supervisor

Paul A. Goud

Dr. Paul A. Goud, Co-Supervisor

I. Filanovsky

Dr. Igor Filanovsky, Internal Examiner

Z. J. Koles

Dr. Zoltan J. Koles, External Examiner

Date: 8 Oct. 97

DEDICATION

I dedicate this thesis to my parents, brother, sister, and friends,

for their love, support and encouragement.

In memory of my grandmother.

ABSTRACT

This thesis discusses the performance of a standard uplink IS-95 CDMA transmission system employing adaptive antenna techniques for suppressing interference in a single cell microcellular environment with 100% voice activity. Fading rates of 10Hz and 100Hz, the resolvable and the unresolvable multipath cases, as well as non-RAKE and RAKE reception cases are investigated. Three types of algorithms are considered: recursive least squares (RLS) and two modified forms of the recursive adaptive beamforming (RAB). A single-antenna and a dual-antenna receiver are also considered for comparison purposes. Simulation results show that a linear adaptive antenna array with eight array elements achieves at least double the capacity gain of the current IS-95 dual-antenna RAKE receiver with the use of feedback-previous-decision approach. The RLS algorithm outperforms both RAB algorithms slightly, but the RLS algorithm is phase-dependent and requires precise phase tracking. Both RAB algorithms converge faster than the RLS algorithm.

ACKNOWLEDGMENTS

First and foremost, I am thankful to God, the most gracious and most merciful, for helping me finish this thesis. My sincere thanks are also given to my family for their continuing support, love, and encouragement.

I would like to express my sincere gratitude to Dr. Colin G. Englefield for introducing me to the field of Wireless Communications and to my supervisors, Dr. Witold A. Krzymien and Dr. Paul A. Goud, for their capable supervision, patience and encouragement throughout my graduate program. I am also grateful to the members of my examining committee, Dr. I. Filanovsky and Dr. Z. Koles, for reviewing this thesis.

It is my pleasure to thank Songsong Sun and Peng Mok for many helpful discussions. My thanks are also due to the TR*Labs* students, especially Kwok Sing Cheng and Endymion Bun Yeung, for providing a pleasure working environment. My appreciation is given to Mr. Ngu and his family, who have made Edmonton "home" to me for many years.

Finally, I am indebted to Telecommunications Research Laboratories (TR*Labs*) for providing me with research facilities and financial assistance for my M.Sc. program.

Table of Contents

1. INTRODUCTION **1**
- 1.1 Wireless Personal Communication 1
- 1.2 Project Motivation 5
- 1.3 The IS-95 Standard 6
  - 1.3.1 Forward link 7
  - 1.3.2 Reverse link 8
  - 1.3.3 Power control 10
- 1.4 Radio Propagation Channel 11
  - 1.4.1 Average path loss 12
  - 1.4.2 Large-scale fading 12
  - 1.4.3 Small-scale fading 12
  - 1.4.4 Delay spread 14
  - 1.4.4 Noise 14
- 1.5 Countermeasures to Channel Distortion 15
  - 1.5.1 Error control coding 15
  - 1.5.2 Multi-user detection techniques 15
  - 1.5.3 RAKE receiver 16
  - 1.5.4 Diversity techniques 17
- 1.6 Thesis Overview 20

2. CHANNEL AND SYSTEM MODEL **22**
- 2.1 Outdoor Radio Channel 22
  - 2.1.1 Channel model for omni-directional antenna 22
  - 2.1.2 Channel model for linear antenna array 24
- 2.2 Reverse Link Model 27
  - 2.2.1 Transmitter model 27
  - 2.2.2 Omni-directional antenna receiver model 28
  - 2.2.3 Antenna array receiver model 31
  - 2.2.4 Power control model 37
- 2.3 Summary 40

3. ADAPTIVE ANTENNA ARRAYS **41**
- 3.1 Theory of a Uniform Linear Array 41
- 3.2 Array Structure and Geometry 45
- 3.3 Adaptive antenna Array Techniques 47
  - 3.3.1 Switched beam system 47
  - 3.3.2 Simple beamformer 48
  - 3.3.3 Subspace-based techniques 51
  - 3.3.4 Eigenfilter techniques 53
  - 3.3.5 Optimum combining techniques 57
- 3.4 Summary 60

4. ADAPTIVE ANTENNA ARRAY ALGORITHMS **62**
- 4.1 IS-95 Antenna Array Structure 62
- 4.2 Recursive Least Squares Algorithm 65
- 4.3 Two Modified Recursive Adaptive Beamforming Algorithms 69
- 4.4 Summary 75

5. SIMULATIONS AND RESULTS 76
5.1 Simulation Methodology 77
5.2 Considerations for Phase-Dependency and Algorithm Parameters 79
5.3 Power Control Parameters for Different Receivers 81
5.4 SINR Distribution for Different Receivers 84
5.5 Radiation Patterns 88
5.6 Rates of Convergence 90
5.7 User Capacity for Different Receivers 93
5.8 Summary 100

6. CONCLUSIONS 101
6.1 Thesis Summary 101
6.2 Future Directions 102

REFERENCES 104

LIST OF TABLES

Table 2.1. Decay constants for power delay profile.....23

Table 5.1(a). Power control parameters ($\bar{\mu}$, σ_s) for different receivers at 10Hz fading rate.....83

Table 5.1(b). Power control parameters ($\bar{\mu}$, σ_s) for different receivers at 100Hz fading rate.....83

Table 5.2(a). SINR distribution for different receivers at 10Hz fading rate.....87

Table 5.2(b). SINR distribution for different receivers at 100Hz fading rate.....87

Table 5.3(a). User capacity for different receivers at 10Hz fading rate.....99

Table 5.3(b). User capacity for different receivers at 100Hz fading rate.....99

LIST OF FIGURES

Figure 1.1. IS-95 mobile transmitter block diagram....8

Figure 1.2. Multipath propagation in urban areas....11

Figure 1.3. Typical variation of received signal strength in a fading channel. 13

Figure 2.1. Diagram of a uniform linear antenna array. 25

Figure 2.2. Non-coherent OQPSK receiver....29

Figure 2.3. IS-95 square law combiner. 30

Figure 3.1. Diagram of a simple beamformer....41

Figure 3.2. Normalized directional gain pattern for an eight-element uniform array....44

Figure 3.3. Radiation patterns formed by different values of interelement spacing....46

Figure 4.1. Linear adaptive antenna array structure. 63

Figure 5.1(a). Probability distribution functions for the output SINRs for 0.1% BER....86

Figure 5.1(b). Average bit error rate for different SINRs....86

Figure 5.2(a). Radiation patterns for the unresolvable multipath case. 89

Figure 5.2(b). Radiation patterns of the fourth spatial filter. 90

Figure 5.3. Rates of Convergence for different 2.5MHz non-RAKE receivers at 10Hz fading rate. 93

Figure 5.4(a). User capacity for different non-RAKE receivers at 10Hz fading rate....95

Figure 5.4(b). User capacity for different non-RAKE receivers at 100 Hz fading rate....95

Figure 5.4(c). User capacity for different RAKE receivers at 10Hz fading rate. 96

Figure 5.4(d). User capacity for different RAKE receivers at 100 Hz fading rate. 97

Figure 5.4(e). User capacity for different fading rates.....98

LIST OF SYMBOLS

a	a constant
a_i	i-th scalar in the initial vector
$a^{(I)}(t)$	I-channel base-specific short PN code
$a^{(Q)}(t)$	Q-channel base-specific short PN code
$\boldsymbol{a}$	vector composed of the array response vectors of the desired signal components
$\hat{\boldsymbol{a}}(n)$	estimated array response vector of the desired signal at the n-th Walsh symbol
$\boldsymbol{a}(\theta)$	array response vector for the angle of arrival θ
$\boldsymbol{a}(\theta_{k,l})$	array response vector for the k-th user and the l-th path
$A_{k,l}(m)$	product of the power control parameter, the fading amplitude and the phase for the k-th user and the l-th path
$\boldsymbol{A}$	a given matrix
$\alpha_{k,l}(t)$	instantaneous fading amplitude for the k-th user and the l-th path
b	a constant
$\boldsymbol{B}$	$V \times V$ positive-definite matrix
β	reference signal magnitude
c	speed of light
$c_k(t)$	user-specific long PN code
$c_k^{(I)}(t)$	product of the user's PN code and the I channel PN-codes
$c_k^{(Q)}(t)$	product of the user's PN code and the Q channel PN-codes
d	interelement distance
$^\circ$	degree
δ_0	a small positive scalar

e	exponential function
$e(m)$	error signal at the m-th Walsh element
$\boldsymbol{e}_i$	eigenvector associated with the eigenvalue λ_i
$\boldsymbol{e}_i^s$	signal eigenvector
$\boldsymbol{e}_i^n$	noise eigenvector
E	expected value
E_s	estimated signal energy per Walsh symbol
ε	eigenvector estimation error
ξ	cost function
$\xi(m)$	time-updated version of the cost function
f	f-th branch of the 64-ary outputs
$F(\theta)$	array factor
$\phi_{kl}(t)$	varying phase for the k-th user and the l-th path
Φ	electrical angle
$\overline{\Phi}$	ensemble-average product vector
$\Phi(m)$	V-by-1 time-updated version of the ensemble-average product vector $\overline{\Phi}$
g	an index
$G(\theta)$	normalized directional antenna gain pattern
γ	a scalar
h	transmitted Walsh symbol value
$\hat{h}$	estimated Walsh symbol value
$h_k(t)$	channel impulse response for the k-th user
$\boldsymbol{h}_k(t)$	channel impulse response of the antenna array for the k-th user
H	hermitian transpose

$\boldsymbol{i(m)}$	interference term containing the intersymbol and multiuser interference components in the pre-correlation signal vector
$\boldsymbol{i'(n)}$	interference term due to intersymbol and multiuser interference components in the post-correlation signal vector
I	total number of desired and interfering signal components.
$\boldsymbol{I}$	identity matrix
j	complex number of $\sqrt{-1}$
k	k-th user
K	total number of users
$\boldsymbol{K}$	$V \times V$ positive-definite matrix
$\boldsymbol{K(m)}$	Kalman gain vector
l	l-th path
ℓ	number of desired signal components
L	maximum number of paths in the multipath
λ	carrier wavelength
λ_i	i-th eigenvalue
Λ	diagonal matrix
n	n-th Walsh symbol
$\overline{n}^2$	average noise power in the IS-95 power control algorithm
$n_o(t)$	channel noise
n_p	number of Walsh symbols considered in a power control command bit
$\boldsymbol{n_o(t)}$	channel noise vector
$\boldsymbol{n(m)}$	channel noise in the pre-correlation signal vector
$\boldsymbol{n'(n)}$	channel noise in the post-correlation signal vector
$N(t)$	complex envelope of the total noise

η_{max}	dominant eigenvalue of the matrix $\boldsymbol{A}$
m	m-th Walsh element
$\boldsymbol{M}$	a matrix
μ	forgetting factor
$\bar{\mu}$	average power of the desired user
$\boldsymbol{p}$	$V \times 1$ vector
P_i	signal or interference power for the i-th path
$P(\theta)$	conventional beamformer density spectrum
$P(\hat{\tau}_l)$	normalized average power for the l-th path
$\boldsymbol{P}$	a matrix
π	pi
%	percent
$\boldsymbol{Q}$	a matrix
$\hat{\boldsymbol{Q}}(n)$	estimated array interference covariance matrix at the n-th Walsh symbol
$\boldsymbol{Q}(n)$	array interference covariance matrix
$\boldsymbol{Q}_{xx}(n)$	array interference covariance matrix in the pre-correlation array covariance matrix
$\boldsymbol{Q}_{zz}(n)$	array interference covariance matrix in the post-correlation array covariance matrix
$r_o(m)$	reference signal at the m-th Walsh element
$r(t)$	total received complex baseband noisy signal
$\boldsymbol{r}(t)$	complex baseband received signal vector

$r_k(t)$	complex baseband received k-th user's signal
$\boldsymbol{R}$	auto-correlation matrix of a received array signal vector
$\boldsymbol{R}_{xx}(m)$	time-updated version of the auto-correlation matrix of the pre-correlation signal vector $\boldsymbol{x}(m)$
$\boldsymbol{R}_{xx}(n)$	pre-correlation array covariance matrix at the n-th Walsh symbol
$\boldsymbol{R}_{zz}(n)$	post-correlation array covariance matrix
$\overline{\boldsymbol{R}}_{nn}$	ensemble-average array interference covariance matrix
$\overline{\boldsymbol{R}}_{zz}$	ensemble-average of the post-correlation array covariance
$\rho_k(t)$	closed-loop power control parameter
σ_s	associated standard derivation of $\overline{\mu}$
σ_n^2	channel noise power
σ^2	power of the Gaussian noise composed of both ISI and MAI
$s_k(t)$	simplified transmitted complex baseband for the k-th user
$s_k^{RF}(t)$	RF transmitted signal for k-th user
$s(t)$	a single narrowband signal
$S(t)$	complex envelope of the incoming narrowband signal $s(t)$
*	complex conjugate
τ	electrical time delay
τ_d	profile decay constant
τ_l	excess delay for the l-th path
τ_{max}	maximum excess delay

T_c	PN chip period
T_o	half of a PN chip period
T_p	period of the power control command bit
T_w	Walsh element period
Γ	interelement delay
θ	angle of arrival measured counterclockwise from the array axis
$\theta_{k,l}$	azimuth angle of arrival for the k-th user and the l-th path
$\boldsymbol{U}$	an unitary matrix
v	v-th array element
$\boldsymbol{v}_0$	$V \times 1$ initial vector
$\boldsymbol{v}_t$	estimated dominant eigenvector at the t-th iteration
$\hat{\boldsymbol{v}}$	eigenvector corresponding to the dominant eigenvalue η_{max} of the matrix A
V	number of array elements
ς	a scalar in the Weiner filter solution
$\boldsymbol{w}$	complex weights of the spatial filter
$\boldsymbol{w}(m)$	complex weights at the m-th Walsh element.
$W_k^{(h)}(t)$	h-th orthogonal Walsh function (symbol) of the k-th user
$W_r^{(\hat{h})}(n,m)$	$\hat{h}$-th Walsh element sequence at the n-th Walsh symbol and the m-th Walsh element
ω_c	carrier frequency
x	a variable

$x_1(t)$	received signal at the first array element
$x_2(t)$	received signal at the second array element
$x_{kl}(m)$	complex baseband PN-despread signal
$x_{kl}^{(I)}(m)$	in-phase PN-despread signal
$x_{kl}^{(Q)}(m)$	quadrature PN-despread signal
$\boldsymbol{x}(m)$	pre-correlation signal vector
$\boldsymbol{x}_{k,l}(m)$	signal component of the pre-correlation signal vector for the k-th user and the l-th path
$X_1(t)$	complex envelope signals associated with $x_1(t)$
$X_2(t)$	complex envelope signals associated with $x_2(t)$
$y(t)$	weighed array output
$Y(t)$	complex envelope of the weighted array output
$z_{n,f}$	f-th decision value at the output of the IS-95 square-law combiner at the n-th Walsh symbol interval
$\boldsymbol{z}(n)$	post-correlation signal vector

LIST OF ABBREVIATIONS

AMPS	Advanced Mobile Phone Service
AWGN	additive white Gaussian noise
BER	bit error rate
BFN	beamforming network
CDMA	code division multiple access
dB	decibel
DS-CDMA	direct-sequence code division multiple access
FDMA	frequency division multiple access
FM	frequency modulation
FSK	frequency shift keying
GHz	gigahertz
GSM	Global System for Mobile communications
Hz	hertz
i.i.d.	independent and identically distributed
I	in-phase
ISI	intersymbol interference
IS-54	North American Interim Standard
IS-95	Interim Standard-95
kbps	kilo bits per second
kHz	kilohertz
km/hr	kilometers per hour
LPF	low pass filter
ms	millisecond
MAI	multiple access interference

Mchips/sec	mega chips per second
MHz	mega hertz
MMSE	minimum mean-squared error
MTSO	mobile telephone switching office
ns	nanosecond
NMT	Nordic Mobile Telephones
NTT	Nippon Telephone and Telegraph
OQPSK	Offset Quadrature Phase Shift Keying
PDC	Personal Digital Cellular
PE	polynomial expansion
PIC	parallel interference cancellation
PN	pseudo-noise
PRBS	pseudorandom binary sequence
PSTN	public switched telephone network
Q	quadrature
QoS	quality of service
QPSK	Quadrature Phase Shift Keying
rms	root mean square
RAB	recursive adaptive beamforming
RLS	recursive least squares
RF	radio frequency
SIC	successive interference cancellation
SINR	signal-to-interference-and-noise ratio
TACS	Total Access Communications System
TDMA	time division multiple access
XOR	modulo two addition by way of exclusive OR gates
ZF-DF	zero-forcing decision-feedback

1. INTRODUCTION

1.1 Wireless Personal Communication

This century has seen the mature development of a public wireline network which provides reliable and affordable communication of voice and low-rate data around the world. The wireline services no longer satisfy all the needs of many subscribers because of the limitation of a fixed wireline connection to the network. The goal of wireless communication is to allow mobile subscribers access to the capabilities of the global wireline telephone network wherever wireless communication coverage is provided. With the development of the cellular concept in the 1960s and of the highly reliable, miniature, solid-state radio frequency hardware in the late 1970s, the wireless communications era was born with the growth of wireless communications, it is expected that there will be an equal number of wireless and conventional wireline customers throughout the world by the first couple of decades of the 21st century [1]. However, the available radio frequency spectrum is limited, and hence must be regulated by governments and international agencies. In order to meet the increasing demand for mobile service, it becomes imperative to restructure the wireless communication system to achieve high user capacity with limited radio spectrum.

The cellular concept allows the reuse of the limited radio spectrum to achieve a much higher subscriber density per MHz of spectrum. The whole service area is covered by a large number of small area cells. The whole available frequency spectrum is divided into multiple radio frequency (RF) channels. Each cell is allocated a subset of all available

RF channels and the same set of channels is reused in every other cell cluster. The first-generation cellular systems were introduced in 1980s in analog form. Various standard systems were developed worldwide such as NTT (Nippon Telephone and Telegraph) systems in Japan, TACS (Total Access Communications System) in United Kingdom, and NMT (Nordic Mobile Telephones) in European countries. In North America, research on cellular system was pioneered by Bell Laboratories during '70s, and the initial implementation of the first-generation North-American analog cellular system is known as Advanced Mobile Phone Service (AMPS). AMPS cellular service has been available to public since 1983. All analog cellular systems use frequency modulation (FM) for speech transmission, frequency shift keying (FSK) for signaling, and frequency division multiple access (FDMA) to enable subscribers access to the network. In the AMPS standard, the typical frequency reuse plan employs a 7-cell cluster with three sectors per cell and each active user is assigned a 30-kHz channel. However, inadequate capacity and a failure to support new services such as the transmission of data for fax, e-mail and files were the major problems [2,3].

The development of low-rate digital speech coding techniques and continuous advances in integrated circuit fabrication techniques (increasing transistor count per unit area) gave birth to second-generation digital cellular systems such as Global System for Mobile communications (GSM) in Europe and Personal Digital Cellular (PDC) in Japan. In late 1991, the first American digital system, the North American Interim Standard (IS-54), was installed in major United State cities. These second-generation digital cellular systems are based on digital modulation schemes for speech transmission and are a hybrid

of the time division multiple access and the frequency division multiple access achemes (TDMA/FDMA). Each user is assigned a specific frequency/timeslot combination and thus user capacity increases. For example, IS-54 retains the 30-kHz channel spacing of AMPS and each frame in the 30-kHz channel is divided into six timeslots. Each full-rate speech encoder uses two timeslots for transmission. Therefore, IS-54 provides approximately triple the capacity of AMPS. If half-rate speech encoders are introduced, each 30-kHz channel will be able to accommodate six user channels [1,2].

In recent years, another type of second-generation digital cellular system, using direct-sequence code division multiple access (DS-CDMA), has received considerable attention because of its potential for capacity increase. In North America, Interim Standard-95 (IS-95) CDMA systems were introduced in 1993 [1]. In FDMA cellular systems and in TDMA/FDMA systems, since the frequency is reused only outside of the cell, the co-channel multiple access interference (MAI) only comes from other cells. However, DS-CDMA systems apply a universal one-cell frequency reuse pattern. The systems transmit all active user signals simultaneously in the same RF channel in all cells, but each user uses his own pseudo-noise (PN) sequence to create a separate channel. Therefore, approximately half of the MAI on a given frequency band comes from outside cells, but the other half comes from the user traffic within the same cell on the same frequency band. The ratio of the out-of-cell and intra-cell interference depends on the path loss law. Since all users are using the same frequency band, the trunking efficiency improves significantly. However, MAI in CDMA systems is the most dominant factor

limiting traffic capacity, and hence mitigation of the MAI can result in significant capacity gains [4].

The 1.23Mchips/sec IS-95 CDMA standard [5] in the reverse link may employ both space diversity, with two spatially separated antennas and equal gain noncoherent combining (using a dual-antenna receiver), and also time diversity techniques, with multipath noncoherent combining (using a RAKE receiver). The current IS-95 systems have already achieved approximately a double capacity gain by taking advantage of intermittent voice activity [4], and a triple capacity gain through the use of a conventional fixed three-sectored antenna at the cell site [6]. Recently, antenna array reception techniques have been studied extensively to mitigate the multiple access interference and thereby achieve further capacity gains. Antenna array reception techniques, an extension of the conventional fixed three-sectored antenna reception technique, perform spatial filtering to exploit the spatial distribution of mobile users. The antenna array receiver maximizes the signal(s) from some direction(s) of arrival and minimize MAI from other directions. It is shown that directional antennas at the base station can provide dramatic performance improvement on the reverse link, as compared to an omnidirectional receiver [6,7]. Thus, antenna array reception techniques are of interest in this thesis. There are different ways of achieving this improvement, from simple fixed multi-beam schemes to complex steerable adaptive antenna array techniques [8,9].

1.2 Project Motivation

In order to meet the increasing demands of wireless subscribers, the present IS-95 CDMA system must be modified to increase the traffic capacity and improve the quality of service (QoS). Since any cellular radio system is interference limited rather than noise limited, mitigating the MAI is the chief objective.

In this thesis, adaptive antenna array techniques are implemented in a base-station receiver to reduce the MAI, and thus the performance gain of the adaptive antenna array receiver is compared with the current IS-95 dual-antenna RAKE receiver. For additional comparison purposes, several antenna configurations have been considered for the base-station receiver, namely a single antenna, a dual-antenna, and a linear adaptive eight-element antenna array. These different antenna options are applied in the reverse link of a microcellular CDMA system using transmission techniques as specified by the IS-95 standard [5], and operating in the 1.9 GHz band. Performance comparison are carried out for both the 1.25MHz and 2.5MHz system bandwidths. The former case produces an unresolvable multipath scenario while the latter is a resolvable one. Both a non-RAKE and a RAKE receiver using multipath non-coherent combining are analyzed. Fading rates of 10Hz and 100Hz are investigated, which at the 1.9GHz carrier frequency correspond to the mobile velocities of approximately 6 km/hr and 60 km/hr respectively, typical for a pedestrian and an urban vehicular user. For wireless telephony (speech communication), a bit error rate (BER) of 0.1% is required to provide a good quality call, so this criterion is used to determine the user capacity of the system.

The following section presents the IS-95 standard. Section 1.4 discusses the impairments of a radio channel which cause performance degradation in wireless communications and Section 1.5 introduces several techniques which can be used to mitigate the channel impairments. An overview of this research project is presented in Section 1.6.

1.3 The IS-95 Standard

In any digital two-way speech communication system, the speech is encoded by a voice encoder (also called vocoder) before transmission. The purpose of speech encoding is to reduce the number of bits required to represent speech. The encoded speech is transmitted to the base station which is connected to the mobile telephone switching office (MTSO) or to the public switched telephone network (PSTN). The link carrying signals from the base-station to the mobile unit is called the downlink or the forward link; the link from the mobile unit to the base-station is called the uplink or the reverse link.

At its full rate, the IS-95 CDMA vocoder generates data at 8.6 kbps. The data are packetized into 20-ms blocks (called frames), and hence each frame has 172 bits. After appending 12 parity bits by a block encoder for error detection, each frame has 184 bits. Then, 8 zero bits are added to each frame (to facilitate convolutional decoding at the receiver), which increases the bit rate to 9.6 kbps. That bit stream is then convolutionally encoded and modulated by different schemes in forward and reverse links.

1.3.1 Forward link

On the forward link, the user basic bit stream (9.6 kbps) is encoded using a rate 1/2 convolutional code, yielding 19.2 kbps. Then, it is interleaved to uniformly disperse the bit error bursts encountered during transmission, and XORed (i.e. added modulo two by way of exclusive OR gates) with a long code serving as a privacy mask. The long code is generated by a pseudorandom binary sequence (PRBS), or called PN code, of period 2^{42}-1 chips. Following the interleaver, the 19.2 kbps sequence is spread using 64-ary Walsh symbols to achieve 1.2288Mchips/sec, which represents a spreading gain of 128 with respect to the original data rate. Each user is spread with a specific Walsh symbol. Since the Walsh matrix has the property that every row is orthogonal to every other row, perfect separation among the different synchronized users in a given cell is achieved, at least for a single-path channel. Quadrature Phase Shift Keying (QPSK) modulation is then used for radio transmission. The data is split into in-phase (I) and quadrature (Q) channels and the data in each channel is XORed with a unique short (or pilot) PRBS of period 2^{15} chips in order to reduce interference between mobiles that use the same Walsh sequence in different cells and to provide the desired wideband spectral characteristic (not all of the Walsh functions yield a wideband power spectrum). Orthogonality among users within a cell is achieved because their signals are spread synchronously. Nevertheless, the orthogonalization is not preserved between different paths in a multipath propagation channel, and among the forward links of different cells.

To provide coherent detection at the mobile station receiver, a pilot signal is transmitted and used as a coherent phase reference in each cell. The pilot signal in each

cell is made up of the same short PRBS and is transmitted at higher power than the user signal. Typically 20% of the total base station transmitted power is allocated to the pilot signal. Each cell uses a different time offset on the short codes and thus IS-95 systems are allowed to reuse all 64 Walsh codes in all other cells [2,10].

1.3.2 Reverse link

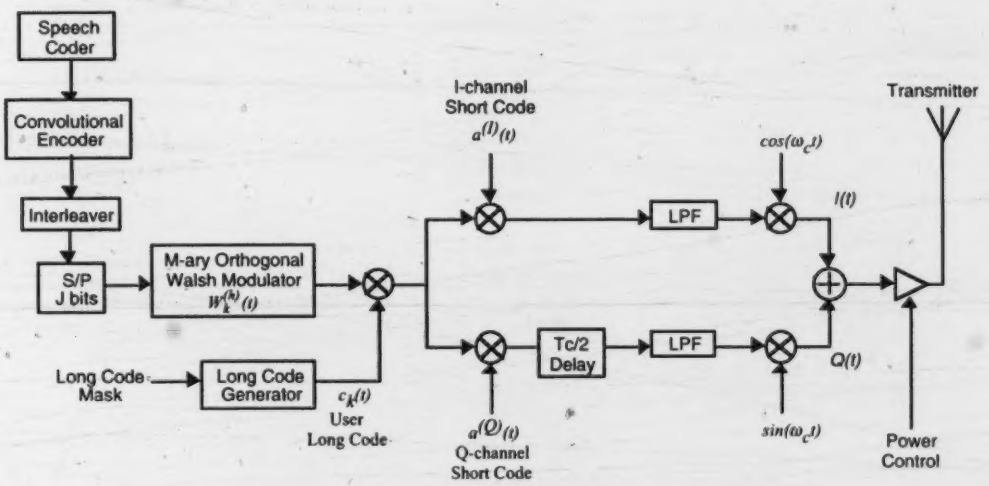

Figure 1.1. IS-95 mobile transmitter block diagram.

On the reverse link, since the mobile station cannot afford the power of a pilot signal, a different spreading strategy is used. The IS-95 mobile transmitter block diagram is shown in Figure 1.1. The voice calls are assumed to be transmitted at 9.6kbps. The voice call of 9.6kbps is first packetized into 20ms frames. Each block is 1/3-convolutionally encoded resulting 28.8kbps. After interleaving, each 6 encoded symbols are mapped into corresponding 64-ary orthogonal Walsh symbols. The 1/3 coding and the mapping onto Walsh symbols result in a greater tolerance to interference. After Walsh symbol mapping, the data rate is 307.2kbps. The 64-ary modulation generates 96 Walsh

symbols per 20ms frame and each Walsh symbol consists of 64 Walsh elements. The resulting Walsh chip sequence is then spread by a user-specific long pseudo-noise (PN) code of 1.2288Mchips/sec, which is unique for each mobile unit in the system (each Walsh element is spread by a factor of four). As a result, the final chip rate is 1.2288Mchips/sec. Since the long codes are applied after the use of the 64-ary Walsh modulation, the reverse link signals are not orthogonal. The spread data stream is then split into in-phase(I) and quadrature(Q) channels and multiplied by two separate short cell-specific PN codes which are same for all users in the same cell. The Q channel data stream is delayed by half of a PN chip period to achieve Offset Quadrature Phase Shift Keying (OQPSK) modulation for mitigating envelope transients inherent to Quadrature Phase Shift Keying. After baseband filtering, the spread signals are power-controlled and upconverted to radio frequency for transmission. A 1.25MHz frequency slot is allocated for transmission. In the modified 2.5MHz system, eightfold instead of fourfold spreading of Walsh elements is applied after the 64-ary modulation (i.e. each Walsh element is spread by eight PN chips).

Because of the absence of the pilot signal, the IS-95 base-station employs non-coherent receivers. Due to the non-orthogonality among in-cell users and non-coherent detection, the reverse link normally limits the system capacity, and hence its improvement is desirable [2,10]. Thus, the implementation of the adaptive antenna array in the reverse link is of interest.

1.3.3 Power control

The MAI due to near/far problem is a major problem in CDMA systems. This interference is due to the nonzero cross-correlation of the spreading sequences assigned to individual users. A desired lower-power user may be overwhelmed by the very strong undesired user's signal, since users near the receiver are received at higher power than those far away, and those farther away suffer a degradation in performance. Even if users are at the same distance, there can be an effective near/far effect because some users may be received during a deep fade. Therefore, tight power control of transmit power is very important for DS-CDMA, which attempts to ensure that all signals from the mobiles within a given cell arrive at the base station with approximately the same and adequate power. The primary use of power control is to maximize the total user capacity; an additional benefit is to minimize the power consumption of a portable unit. Both open-loop and closed-loop power control schemes are used. Open-loop power control is based on the similarity of loss in the forward and reverse paths and normally used in forward link. The received power at the mobile station is used as a reference to adjust the transmitted power to the mobiles that suffer from excessive intercell interference at the cell boundary. Closed-loop power control is used to force the power from the mobile station to deviate from the open-loop setting and done by an active feedback system from the base station to the mobile unit. Both open and closed-loop power control are used in the reverse link, and it must be fast enough to compensate for small-scale fading of fast moving vehicles, as well as changes in shadowing [2,4,10].

1.4 Radio Propagation Channel

When a mobile unit moves through a coverage area, each transmitted signal ray may undergo reflection, diffraction, and scattering in the presence of buildings, mountains and foliage, etc. Figure 1.2 shows the mechanism for multipath propagation in an urban environment. Each replica of the original transmitted signal reaches the receiver with a different propagation delay, attenuation, and angle of arrival. The radio multipath propagation channel is complex and places fundamental limitations on the performance of wireless communication systems. The strength of each wave decreases as the distance between the transmitter and receiver increases. The instantaneous signal power varies due to the motion of a mobile or of surrounding objects. The received signal may be distorted due to the time dispersion and background noise. On the other hand, without multipath propagation, the mobile wireless communication would be impossible because of the absence of a line-of-sight path in a typical urban environment. In fact, the reflected, diffracted and scattered signals maintains the continuity of a transmission link.

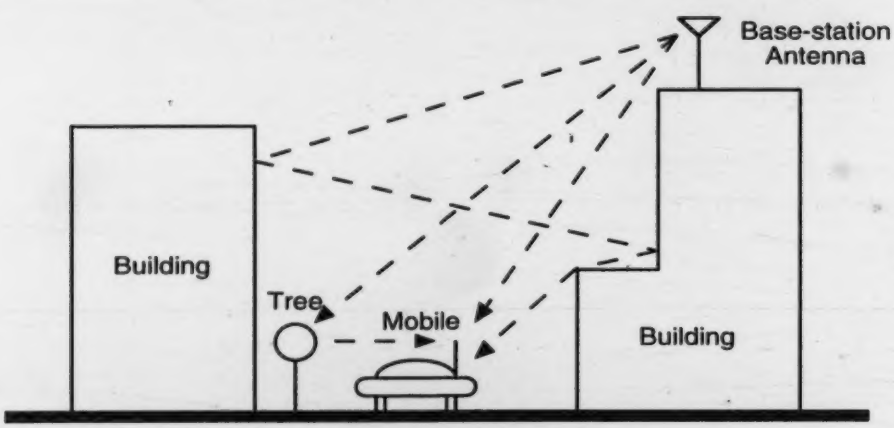

Figure 1.2. Multipath propagation in urban areas.

1.4.1 Average path loss

Average path loss is generally the essential parameter in determining the amount of received power that is expected at a particular distance or location from a transmitter, and it determines fundamental parameters such as transmitter power requirements, coverage area, and battery life. The average received signal power decreases with an increase in the separation between the transmitter and receiver.

1.4.2 Large-scale fading

There are two types of fading in a mobile radio environment: large-scale fading and small-scale fading. Large-scale fading is caused by shadowing effects of the surrounding environmental clutter, such as large geographical or man-made obstacles, located between the transmitting and receiving ends of communication link. The measured received signals with the same separation between the transmitter and receiver is log-normally distributed.

1.4.3 Small-scale fading

Small-scale fading occurs because the received multipath signal is a superposition of several replicas, which interfere either constructively or destructively. Due to the motion of the mobile or of the surrounding objects, the relative phase of each component of the multipath signal is changing continually and thus the instantaneously received signal will fluctuate rapidly. When a dominant non-fading component caused by line-of-sight propagation exists, small-scale fading can be modeled by a Rician distribution. However, in a typical urban environment, a line-of-sight path seldom exists and signals normally arrive at the receiver via indirect paths. When a direct path is absent, small-scale fading is modeled by a Rayleigh distribution. The fading rate is directly related to the

Doppler shift caused by the motion of the mobile and of the surroundings. If the mobile moves faster than the surrounding objects, only the speed of mobile need be considered. Figure 1.3 illustrates the Rayleigh fading of a mobile radio channel at a walking speed of 6 km/hr and at a vehicular speed of 60 km/hr, at a carrier frequency of 1.9GHz. The fading rate increases proportionally to the speed of the mobile and the received signal power may vary by as much as 40 dB when the mobile moves by only a fraction of a wavelength [11].

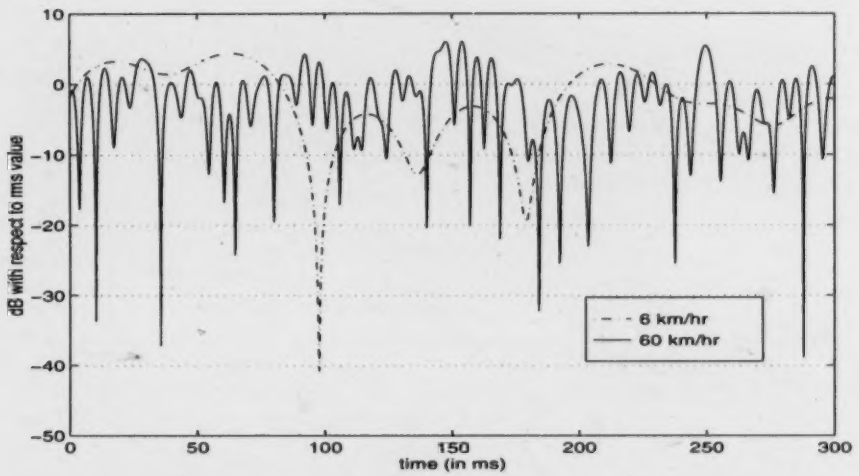

Figure 1.3. Typical variation of received signal strength in a fading channel.

In CDMA, the Rayleigh fading effect is less prqnounced because the chip rate is so high that fewer multipath signals from one transmitted chip arrive during one chip duration (resolution of different paths is better in a wideband system). The base station receiver can detect the desired signal properly while rejecting its other multipath components [2,4]. However, in a typical urban environment, due to the presence of closely-spaced scatterers, the fading still occurs.

1.4.4 Delay spread

Time dispersion arises due to multipath propagation. A time delay associated with each path is a function of the path length. When multipath delays approach or exceed the symbol period, the spreading or smearing of signal will result. In digital transmission, the received symbol is distorted by the overlapping of the delayed multipath symbols, producing intersymbol interference (ISI) or also called self-multipath interference. The root mean square (rms) delay spread of a channel is a measure of the multipath spreading in different wireless environments. When the rms delay spread of a channel is greater than about 10% of a chip period, the channel is called a time dispersive channel or a frequency selective channel because different frequency components of the signal experience uncorrelated attenuation [1,11]. The CDMA propagation channel is frequency selective because of a shorter chip period. RAKE receivers can be used to resolve and combine time dispersive multipath components in order to combat the small-scale fading significantly.

1.4.5 Noise

In any wireless communication channel, noise is omni-present. External noise includes galactic noise, automobile ignition noise and noise generated by lightning, electric motors, etc. Internal noise is normally equivalent to thermal noise generated by all electronic components in the receiver itself. The combination of the external noise and the internal noise is generally modeled as additive white Gaussian noise (AWGN). However, mobile multi-user radio systems tend to be multiple access interference limited rather than noise limited because the noise effects are often insignificant compared to the signal levels

of co-channel users. The ratio of signal strength to the interference and the overall noise is called the signal-to-interference-and-noise ratio (SINR). It is a basic measure of the signal quality.

1.5 Countermeasures to Channel Distortion

Mobile communication systems require various signal processing techniques to mitigate impairments in the hostile mobile radio environment. The techniques include error control coding, multi-user detection, RAKE receiver, and diversity techniques.

1.5.1 Error control coding

Channel coding is used by the receiver to detect or correct some (or all) of the errors introduced by the channel. The added parity bits reduce the information transmission rate. Analog systems may require that the desired signal's average power be at least 18 dB above any noise and interference on the same channel to ensure acceptable call quality. Due to powerful error control coding (both block and convolutional) used on both links of the IS-95 system, normally about 5 dB of average SINR is required to ensure comparable call quality [12].

1.5.2 Multi-user detection techniques

Multi-user detection techniques have been extensively researched recently to mitigate the MAI. Multi-user detectors are not like the conventional matched filter detectors which consider other user signals as noise or interference, but they consider other signals as jointly detected user signals to better detect each individual user. Since the

base station must detect all mobile signals, the base station has knowledge of the chip sequences and timing information of multiple users. The multi-user detector could be implemented at the base station receiver to improve the performance of the reverse link which limits the overall system capacity. However, the optimum multi-user sequence detector is too complex to implement for practical CDMA systems. Many simpler suboptimal multi-user detectors have been proposed in the last few years. Most of the detectors fall into two categories: linear and subtractive interference cancellation. Linear multi-user detectors, such as decorrelating, minimum mean-squared error (MMSE), and polynomial expansion (PE) detectors, apply a linear transformation to the outputs of the matched filter bank to reduce the MAI seen by each user. Subtractive interference cancellation detectors which include the successive interference cancellation (SIC), parallel interference cancellation (PIC), and zero-forcing decision-feedback (ZF-DF) detectors attempt to estimate and subtract off the MAI. These suboptimal multi-user detectors are well understood by now. The next stages of investigation, involving implementation and robustness issues, will lead to determination of the practical and economic feasibility of the multi-user detector [13,14].

1.5.3 RAKE receiver

The performance of a digital transmission system is often degraded by intersymbol interference caused by time dispersive channels. In TDMA systems, the intersymbol interference sets a limit on the transmission rate of the digital radio channel, so a linear or a non-linear equalization may be used at the receiver to combat the intersymbol interference. However, due to the very low correlation between successive

PN chips of CDMA systems, the multipath components delayed in time by more than a chip duration appear like uncorrelated noise or MAI at a receiver, and equalization is not required. On the other hand, since there is useful information in time dispersive multipath components, RAKE receivers can be used to resolve and combine the multipath components in order to reduce the fading amplitude, significantly improving the SINR at the receiver [1,2]. The RAKE receiver is essentially a diversity receiver designed specifically for CDMA systems, where diversity is provided by the fact that the multipath components are practically uncorrelated from one another when their relative propagation delays exceed a chip period.

1.5.4 Diversity techniques

Diversity is a powerful technique to provide wireless CDMA uplink improvement at relatively low cost and to combat fading. The basic principle of diversity techniques is to exploit the random nature of the radio propagation by finding independent or at least weakly corrected signal paths for communications. If one radio path undergoes a deep fade or a deep shadow, another independent path may have a strong signal, so the communication link can be maintained at an acceptable quality. There are two types of diversity: macroscopic and microscopic. Large-scale spatial diversity is the former. It employs multiple receiving antennas located at different base-stations to reduce large-scale fading. On the other hand, microscopic diversity, which requires two or more antennas or frequencies at the same base-station, is used to counteract small-scale fading.

There are six different types of microscopic diversity: space, frequency, time, polarization, field component and angle diversity. Space diversity employs two or more antennas which are separated from each other far enough to receive an independent fading signal in each antenna or diversity branch. A dual-antenna receiver employs two antennas in the base station. Frequency diversity uses two different frequency carriers to transmit the same information with adequate frequency separation for providing independent fading paths. Similarly, time diversity transmits identical messages at time spacings that exceed the coherent time of the channel. Since the CDMA propagation channel is a frequency selective channel in an outdoor urban environment, a RAKE receiver, a special form of time diversity, can be used to exploit the time-delayed multipath signals. Polarization diversity makes use of the two independent fading paths created by the two orthogonally polarized electromagnetic wave components. In fading fields, the electric and the magnetic fields fade independently, but the total electromagnetic energy density remains constant. Field-component diversity employs an antenna system which is capable of separating and combining the electric and the magnetic fields appropriately. Unfortunately, such a system can be used only at low frequencies [15]. Angle diversity (directional diversity), the last microscopic diversity scheme, not only provides independent fading paths but also mitigates the MAI significantly. When a conventional three-sector beam system is employed in the base station receiver, each beam covers a 120° sector. Each sector tracks the desired signal components with different angles of arrival and thus the independent fading paths can be obtained. Unlike an omni-directional

antenna which receives all the incoming signals from all directions with equal antenna gain, the three-sector beam system mitigates the MAI approximately by a factor of three [6]. If smart antennas are employed in the base station receiver, both the beam and the nulls of the antenna array are steerable, and thus the MAI is significantly reduced and the user capacity increases. The details will be explained in Section 3.3.

Signals from diversity branches may be processed using four different diversity combining techniques: selection diversity, switched diversity, maximum ratio combining, and equal-gain combining. In selection diversity, the received signal from each diversity branch is continuously monitored by each receiver and the best signal among the diversity branches is selected. This technique may require a receiver for each diversity branch. However, only one receiver is required for switched diversity. When the current diversity signal falls below a predetermined threshold, the receiver is switched to the next branch in fixed sequence until it finds a signal above the threshold. In the two-branch system, the switch will either stay in the new branch (switch and stay combining [16]) or revert back to the original branch if the newly selected branch is below threshold. Since both selection diversity and switched diversity utilize the signal from only one diversity branch at a time, true combining techniques are better used for further improvement. The best coherent combining technique is the maximum ratio combining in which individual diversity signals are co-phased and weighted in proportion to their SINRs to achieve a maximum output SINR. However, in practice, it is difficult to achieve because of the requirement of correct weighting factors. In equal gain combining, the implementation complexity is drastically reduced because the weighting factor in all branches is the same.

All diversity signals are summed either coherently or non-coherently with equal gain [15]. In IS-95 uplink system, all diversity branches are non-coherently combined with equal gain. The in-phase and quadrature outputs of each branch of the 64-ary correlators are squared separately and then the squared outputs of all diversity branches are summed with equal gain. This non-coherent equal gain combining method is known as the square law combining.

The current IS-95 system has employed a dual-antenna RAKE receiver with non-coherent square-law combining at the base station to enhance the user capacity. Recently, smart antennas, capable of forming directional beam(s) toward the desired signal(s) and placing nulls towards the interfering signals, have been the subject of a significant research effort.

1.6 Thesis Overview

The objective of this research project is to investigate the performance of an adaptive antenna array employed at the base station in the multipath fading outdoor channel on the IS-95 reverse link. Specifically, the RLS algorithm [17] and two modified forms of recursive adaptive beamforming [18] are used to govern the adaptation of the spatial filter of the antenna array. These algorithms achieve an optimum spatial filter solution which forms the main lobe towards the desired signal and places nulls towards the interference. A single-antenna, a dual-antenna, and an adaptive antenna array receiver are studied for comparison purposes, at fading rates of 10Hz and 100Hz. Both the non-

RAKE and the RAKE reception cases as well as the 1.25MHz and the 2.5MHz system bandwidths are investigated. The performance of different receivers is evaluated through extensive computer simulations. The study is presented in the following order.

- Chapter 2 details the channel, the mobile transmitter and the base-station receiver models. A typical IS-95 power control algorithm is also presented.
- Chapter 3 explains the basic concept of the antenna array receiver, the array structure, and the array geometry. Different techniques for determining the spatial filter solution of the antenna array are also surveyed.
- Chapter 4 presents the derivation of the recursive least squares algorithm and the two modified forms of recursive adaptive beamforming.
- Chapter 5 discusses details of the simulation and presents their results.
- Finally, Chapter 6 gives conclusions drawn from the results of the research and discusses possible future work.

2. CHANNEL AND SYSTEM MODEL

This chapter is concerned with the modeling of the channel, the mobile transmitter, the base-station receiver, and the power control. The expression for modeling the desired signal and interference in Walsh element forms used in the simulation is also given.

2.1 Outdoor Radio Channel

Although the channel impulse response is random due to the three basic propagation mechanisms (diffraction, reflection and scattering), the multipath channel impulse response of each user can be written in the form of a tapped delay line model. In this section, channel models for both an omni-directional antenna and a uniform antenna array will be defined. Channel parameters such as the phase, the angle of arrival and the amplitude of each path are chosen specifically for the outdoor, low antenna, urban high-rise environment.

2.1.1 Channel model for omni-directional antenna

When the base-station employs a single antenna to receive the incoming signal, the channel impulse response for the k-th user is :

$$h_k(t) = \sum_{l=1}^{L} \alpha_{k,l}(t)\, \delta(t-\tau_l)\, e^{-j\phi_{k,l}(t)} \qquad (2.1)$$

where $\phi_{k,l}(t)$ is the uniformly distributed over $[0,2\pi]$ phase for the k-th user and the l-th path, $\alpha_{k,l}(t)$ is the instantaneous fading amplitude, L is the maximum number of paths in the multipath, and τ_l is the excess delay for the l-th path, assumed here to be

deterministically and equally spaced over the interval [0, τ_{max}], where τ_{max} is the maximum excess delay.

The choice of the channel parameters, $\alpha_{kl}(t)$ and τ_l, is made to reasonably reflect microcellular propagation conditions (specifically for the outdoor, low antenna, urban high-rise environment), as specified by the JTC RF channel characterization document [19]. The normalized average power delay profile $P(\tau_l)$ of the channel impulse response is assumed to be exponentially decaying:

$$P(\tau_l) = e^{-\tau_l/\tau_d} \tag{2.2}$$

where τ_d is the profile decay constant.

Due to the large amount of variability of delay spread within the chosen environment, three types of channels specified for the chosen environment by [19] are normally considered:

Table 2.1. Decay constants for power delay profile.

Type of Channel	Probability of Occurrence (%)	Decay Constant τ_d (ns)	rms delay spread (ns)
A	40%	140	100
B	55%	750	750
C	5%	2000	1800
Weighted average	100%	568.5	290

The decay constant is proportional to the delay spread of the channel profile. Channel A is the small delay spread case that occurs frequently. Channel B is a medium

delay spread case which also occurs frequently. Channel C is the large delay spread case that occurs only rarely. The chosen profile decay constant has been assumed to be equal to the weighted average of the decay constants; hence, τ_d = 568.5 ns. Four propagation paths are assumed and the temporal separation between adjacent paths has been assumed constant, equal to 407 ns. The first path in the profile is Ricean distributed (with the Rice factor = 1), and the other three are Rayleigh. Thus, the normalized power distribution of the four paths is 0 dB, -6.2 dB, -9.2 dB, and -12.3 dB and they are located at 0 ns, 407 ns, 814 ns, and 1221 ns respectively.

The assumed channel multipath delay profile reasonably reflects the average situation for the considered environment, and at the same time introduces temporal separation equal to only one half of the chip time in the 1.23Mchip/sec IS-95 system. Hence, the results produced by the work give an indication of expected performance of a relatively narrowband, 1.23Mchip/sec IS-95 system in a microcellular setting; with the chip time of as much as 813 ns, the individual paths in the multipath profile are not fully resolvable, which implies a performance loss in comparison with a larger bandwidth system (for the assumed propagation environment, at least 2.5 MHz), which would be able to resolve and combine all significant paths in the profile.

2.1.2 Channel model for linear antenna array

An antenna array contains several antennas spaced closely together. Signals received by antenna array elements are correlated. When a uniform linear antenna array is used in the base-station receiver, array elements are distributed linearly with the same

interelement spacing between adjacent array elements. The uniform linear antenna array is shown in Figure 2.1.

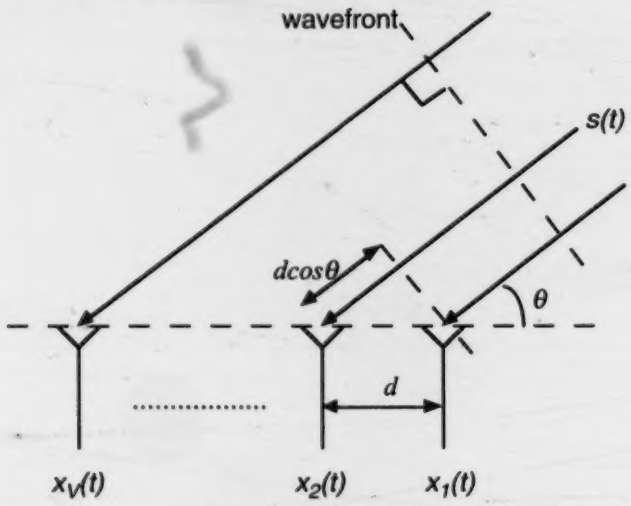

Figure 2.1. Diagram of a uniform linear antenna array.

Suppose that a single incoming signal $s(t)$ arrives at the array with azimuth arrival angle θ measured counterclockwise from the array axis as shown in Figure 2.1. Let V be the number of array elements, d denote the interelement distance and c represent the velocity of radio wave propagation (i.e. speed of light). The output $x_2(t)$ at the second array element is delayed by the time required for the plane wave to propagate through the distance length of $d \cdot \cos\theta$. This interelement delay Γ is given by

$$\Gamma = \frac{d\cos\theta}{c} \tag{2.3}$$

Therefore, the outputs $x_2(t)$ and $x_1(t)$ are related as follows:

$$x_2(t) = x_1(t - \Gamma) \tag{2.4}$$

Since the spread signal bandwidth of the IS-95 CDMA system is very small compared to the carrier frequency ω_c (i.e. it is narrowband signal), the narrowband assumption for antenna array is valid. This enables modeling time delays due to propagation across the array as phase shifts. Since $c = \lambda\omega_c / 2\pi$, the equation (2.4) can be represented by a complex notation.

$$X_2(t) = X_1(t)\exp(\frac{-j\omega_c d\cos\theta}{c}) = X_1(t)\exp(\frac{-j2\pi d\cos\theta}{\lambda}) \qquad (2.5)$$

where $X_2(t)$ and $X_1(t)$ represent the corresponding complex envelope signals associated with $x_2(t)$ and $x_1(t)$. λ is carrier wavelength. If interelement spacing is $\lambda/2$, the above equation is reduced to:

$$X_2(t) = X_1(t)\exp(-j\pi\cos\theta) \qquad (2.6)$$

The signal output at any sensor element can be represented as a time-delayed or time-advanced version of its complex envelope at a reference element $X_1(t)$, a time-delayed or time-advanced version depending on the angle of arrival θ [20].

The response vector of the cell site antenna array to the k-th user and l-th path signal can be organized in a $V \times 1$ vector form, called array response vector. The vector is normalized to 1. The array response vector with uniform half-wavelength interelement separation is:

$$a(\theta_{kl}) = \frac{1}{\sqrt{V}}\,[1,\ exp(-j\pi\cos\theta_{kl}),\ \ldots,\ exp(-j(V-1)\pi\cos\theta_{kl})]^T \qquad (2.7)$$

where θ_{kl} is the azimuth angle of arrival uniformly distributed over [0, π], T is the transpose, and V is the total number of array elements. The channel impulse response of the antenna array can be represented by the following vector.

$$h_k(t) = \sum_{l=1}^{L} \alpha_{kl}(t)\, \delta(t-\tau_l)\, e^{-j\phi_{kl}(t)} a(\theta_{kl}) \tag{2.8}$$

2.2 Reverse Link Model

The models of both the mobile transmitter and two base-station receivers in the reverse link are given. The base-station receivers are an omni-directional and an antenna array receiver. The power control models of the desired signal user and of the interfering user are also presented.

2.2.1 Transmitter model

The IS-95 uplink transmitted signal has been described in Section 1.3.2. To simplify the analysis, baseband filtering is not simulated as specified in the IS-95 standard. The RF transmitted signal for k-th user is:

$$s_k^{RF}(t) = \rho_k(t)\Big[W_k^{(h)}(t)c_k(t)a^{(I)}(t)\cos(\omega_c t) + W_k^{(h)}(t-T_o)c_k(t-T_o)a^{(Q)}(t-T_o)\sin(\omega_c t)\Big] \tag{2.9}$$

where T_o is half of a PN chip period, $c_k(t)$ is a user-specific long PN code, $a^{(I)}(t)$ is the I-channel base-specific short PN code, $a^{(Q)}(t)$ is the Q-channel base-specific short PN code, $W_k^{(h)}(t)$ is the h-th orthogonal Walsh function (symbol) of the k-th user and contains 64

Walsh elements, h is the transmitted Walsh symbol value which is to be detected by the receiver, ω_c is the carrier frequency, and $\rho_k(t)$ is the closed-loop power control parameter. $c_k(t)$, $a^{(I)}(t)$, and $a^{(Q)}(t)$ are assumed to be independent and identically distributed (i.i.d.) random variables taking values ±1 with equal probability in the interval of $[0,T_c]$; each Walsh element in $W_k^{(h)}(t)$ can be +1 or -1 over $[0,T_w]$. In the 1.25MHz system, $T_w=4T_c$, while in the 2.5MHz system, $T_w=8T_c$.

For simplicity, we denote the product of the user's PN code and the I or Q channel PN-codes as

$$c_k^{(I)}(t) = c_k(t)a^{(I)}(t) \text{ and } c_k^{(Q)}(t) = c_k(t)a^{(Q)}(t) \tag{2.10}$$

where $c_k^{(I)}(t)$ and $c_k^{(Q)}(t)$ are assumed to be independent and identically distributed (i.i.d.) random variables taking values ±1 with equal probability. Therefore, the simplified transmitted signal represented in complex baseband notation for the k-th user is:

$$s_k(t) = \rho_k(t)\left[W_k^{(h)}(t)c_k^{(I)}(t) - jW_k^{(h)}(t-T_o)c_k^{(Q)}(t-T_o)\right] \tag{2.11}$$

2.2.2 Omni-directional antenna receiver model

Each user's transmitted signal will undergo multipath propagation; therefore, after down-converting from RF to baseband signal, the complex baseband received k-th user's signal $r_k(t)$ for a single omni-directional antenna is the convolution of the k-th transmitted signal and the k-th channel impulse response.

$$r_k(t) = \sum_{l=1}^{L} s_k(t-\tau_l)\alpha_{kl}(t)\, e^{-j\phi_{kl}(t)} \tag{2.12}$$

The total received complex baseband noisy signal $r(t)$ at the base station is the summation of each user's complex baseband received signal and the channel noise $n_o(t)$:

$$r(t) = \sum_{k=1}^{K} r_k(t) + n_o(t) = \sum_{k=1}^{K}\sum_{l=1}^{L} s_k(t-\tau_l)\alpha_{kl}(t)e^{-j\phi_{kl}(t)} + n_o(t) \tag{2.13}$$

where K is the total number of users present in the cell.

In the IS-95 uplink system, the noncoherent OQPSK receiver, shown in Figure 2.2, is employed to extract the k-th user and l-th path signal from the incoming RF signal $r(t)$. The in-phase and quadrature PN-despread signals $x_{kl}^{(I)}(m)$ and $x_{kl}^{(Q)}(m)$ are obtained from the operations of the I-channel and the Q-channel branches respectively.

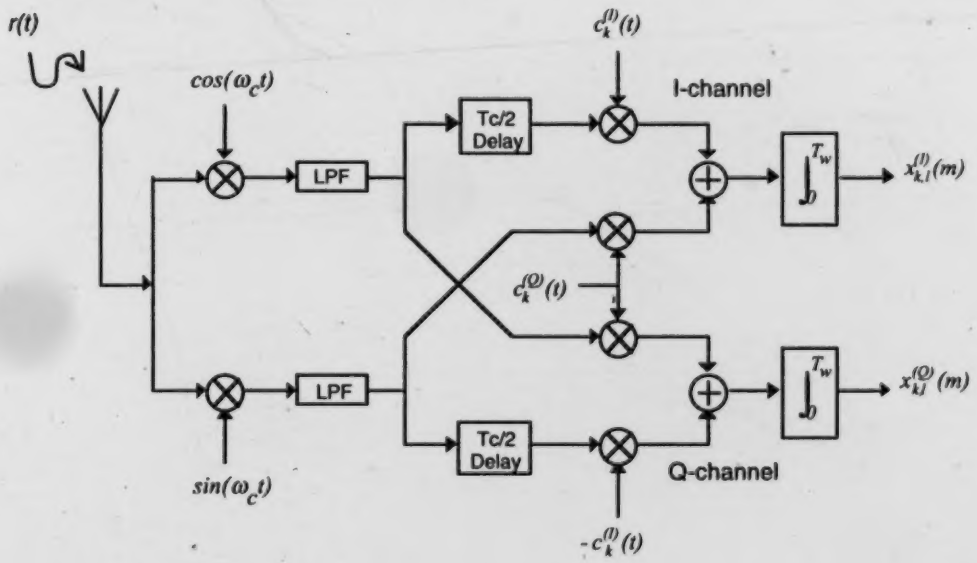

Figure 2.2. Non-coherent OQPSK receiver.

The outputs of the low pass filter (LPF) are correlated (or PN-despread) with the desired user's synchronized PN code in the I-channel and Q-channel separately using the correlation interval sampling of T_w which is 4 PN chips long for the 1.25MHz system and 8 PN chips long for the 2.5MHz system. After the normalization, the resulting digital PN-despread signal in complex baseband notation and in Walsh element form is:

$$x_{kl}(mT_w) = \frac{1}{2T_w}\int_{\tau_l+(m-1)T_w+T_o}^{\tau_l+mT_w+T_o}\left[r(t-T_o)c_k^{(I)}(t-T_o-\tau_l)+ jr(t)c_k^{(Q)}(t-T_o-\tau_l)\right]dt \quad (2.14)$$

The I-channel PN-despread signal is:

$$x_{kl}^{(I)}(m) = Re\left\{x_{kl}(m)\right\} \quad (2.15)$$

and the Q-channel PN-despread signal is:

$$x_{kl}^{(Q)}(m) = Im\left\{x_{kl}(m)\right\} \quad (2.16)$$

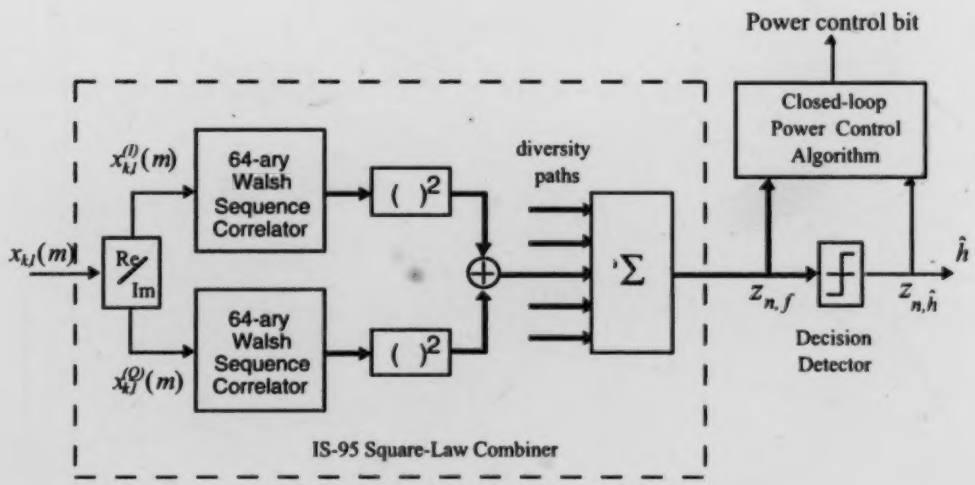

Figure 2.3. IS-95 square law combiner.

Figure 2.3 shows the non-coherent square law combining applied after the IS-95 OQPSK demodulation. The PN-despread signals $x_{kl}^{(I)}(m)$ and $x_{kl}^{(Q)}(m)$ are fed into two separate 64-ary Walsh sequence correlators and then square-law combined. The 64-ary outputs of all diversity branches are added up non-coherently when a RAKE receiver, or a dual-antenna receiver, or both are employed. $z_{n,f}$ is the f-th decision value at the output of the IS-95 square-law combiner at the n-th Walsh symbol interval. The largest value of $z_{n,f}$ is selected in the decision detector in order to determine the transmitted Walsh symbol value h. Finally, the sequence of estimated Walsh symbol values $\hat{h}$ is 64-ary Walsh demodulated, de-interleaved and 1/3-convolutionally decoded. The symbols ^ denote estimates.

2.2.3 Antenna array receiver model

This section defines the model of the linear antenna array with half-wavelength interelement spacing. Similar to equation (2.13), the complex baseband received signal vector $\boldsymbol{r}(t)$ is:

$$\boldsymbol{r}(t) = \sum_{k=1}^{K}\sum_{l=1}^{L} s_k(t-\tau_l)\alpha_{kl}(t)e^{-j\phi_{kl}(t)}\boldsymbol{a}(\theta_{k,l}) + \boldsymbol{n}_o(t) \tag{2.17}$$

where $\boldsymbol{n}_o(t)$ is the channel noise vector with zero mean and covariance.

$$E\{\boldsymbol{n}_o(t_1)\boldsymbol{n}_o(t_2)\} = \sigma_n^2 \boldsymbol{I}\delta(t_1 - t_2) \tag{2.18}$$

where $\boldsymbol{I}$ is the identity matrix and σ_n^2 is the channel noise power. Equation (2.18) implies that the noise is both temporally and spatially white. From equation (2.14), the received

PN-despread signal written in vector notation $x(m)$ is called the pre-correlation signal vector (i.e. the name denotes the signal vector before Walsh sequence correlation). The pre-correlation signal vector for the desired tracked path (i.e. k-th user and l-th path) is:

$$x(m) = \frac{1}{2T_w} \int_{\tau_l+(m-1)T_w+T_o}^{\tau_l+mT_w+T_o} \left[r(t-T_o) c_k^{(I)}(t-T_o-\tau_l) + jr(t) c_k^{(Q)}(t-T_o-\tau_l) \right] dt \qquad (2.19)$$

To reduce or eliminate the need for time intensive simulations, the IS-95 reverse link is simulated Walsh element by Walsh element. The following contains a detailed mathematical analysis which provides expressions for determining the interference of each path in Walsh element by Walsh element form. From equation (2.17), the received complex basband signal of the 2.5MHz system, which is able to resolve all individual paths, can be written as follows:

$$r(t) = s_1(t-t_1)\alpha_{1,1}(t-t_1)e^{-j\phi_{1,1}(t)}a(\theta_{1,1}) + \sum_{l=2}^{L} s_1(t-t_1)\alpha_{1,l}(t-t_1)e^{-j\phi_{1,l}(t)}a(\theta_{1,l})$$

$$+ \sum_{k=2}^{K}\sum_{l=1}^{L} s_k(t-t_1)\alpha_{k,l}(t-t_1)e^{-j\phi_{k,l}(t)}a(\theta_{k,l}) + n_o(t) \qquad (2.20)$$

The first term is the desired path signal vector, the second term is the interference due to self-multipath, the third term is the interference due to other users and the fourth term is the channel noise vector. Since the phase, the amplitude and the power control bit is assumed to be constant over a Walsh symbol, the k-th user and l-th path signal component of the pre-correlation signal vector $x_{k,l}(m)$ is:

$$x_{kl}(m) = A_{kl}(m)a(\theta_{kl})\frac{1}{2T_w}\left[\int_{\tau_1+(m-1)T_w+T_o}^{\tau_1+mT_w+T_o} W_k^{(h)}(t-\tau_1-T_o)c_k^{(I)}(t-\tau_1-T_o)c_l^{(I)}(t-T_o-\tau_1)dt\right.$$

$$-j\int_{\tau_1+(m-1)T_w+T_o}^{\tau_1+mT_w+T_o} W_k^{(h)}(t-2T_o-\tau_1)c_k^{(Q)}(t-2T_o-\tau_1)c_l^{(I)}(t-T_o-\tau_1)dt$$

$$+j\int_{\tau_1+(m-1)T_w+T_o}^{\tau_1+mT_w+T_o} W_k^{(h)}(t-\tau_1)c_k^{(I)}(t-\tau_1)c_l^{(Q)}(t-T_o-\tau_1)dt$$

$$\left.+\int_{\tau_1+(m-1)T_w+T_o}^{\tau_1+mT_w+T_o} W_k^{(h)}(t-T_o-\tau_1)c_k^{(Q)}(t-T_o-\tau_1)c_l^{(Q)}(t-T_o-\tau_1)dt\right] \quad (2.21)$$

$$A_{kl}(m) = \rho_k(mT_w)\alpha_{kl}(mT_w)e^{-j\phi_{kl}(mT_w)} \quad (2.22)$$

For the 2.5MHz system, T_w=8T_c=16T_o. Since each PN chip is assumed to be a rectangular pulse and constant over [0,T_c]; therefore,

$$x_{kl}(m) = A_{kl}(m)a(\theta_{kl})\frac{1}{2T_w}\cdot$$

$$\left[\sum_{i=0}^{7}\int_{\tau_1+(m-1)T_w+iT_c}^{\tau_1+(m-1)T_w+(i+1)T_c} W_k^{(h)}(t-\tau_1-T_o)c_k^{(I)}(t-\tau_1-T_o)c_l^{(I)}(t-T_o-\tau_1)dt\right.$$

$$-j\sum_{i=0}^{15}\int_{\tau_1+(m-1)T_w+iT_o}^{\tau_1+(m-1)T_w+(i+1)T_o} W_k^{(h)}(t-2T_o-\tau_1)c_k^{(Q)}(t-2T_o-\tau_1)c_l^{(I)}(t-T_o-\tau_1)dt$$

$$+j\sum_{i=0}^{15}\int_{\tau_1+(m-1)T_w+iT_o}^{\tau_1+(m-1)T_w+(i+1)T_o} W_k^{(h)}(t-\tau_1)c_k^{(I)}(t-\tau_1)c_l^{(Q)}(t-T_o-\tau_1)dt$$

$$\left.+\sum_{i=0}^{7}\int_{\tau_1+(m-1)T_w+iT_c}^{\tau_1+(m-1)T_w+(i+1)T_c} W_k^{(h)}(t-T_o-\tau_1)c_k^{(Q)}(t-T_o-\tau_1)c_l^{(Q)}(t-T_o-\tau_1)dt\right] \quad (2.23)$$

For the desired signal component (i.e. $k = 1$ and $l = 1$), most of the second term and the third term cancel each other.

$$x_{1,1}(m) = A_{1,1}(m)\boldsymbol{a}(\theta_{1,1})\frac{1}{2T_w}\cdot\Big[T_w W_1^{(h)}(mT_w)$$

$$-j\int_{\tau_1+(m-1)T_w}^{\tau_1+(m-1)T_w+T_o} W_1^{(h)}(t-2T_o-\tau_1)c_1^{(Q)}(t-2T_o-\tau_1)c_1^{(I)}(t-T_o-\tau_1)dt$$

$$+j\int_{\tau_1+(m-1)T_w+15T_o}^{\tau_1+(m-1)T_w+16T_o} W_1^{(h)}(t-\tau_1)c_1^{(I)}(t-\tau_1)c_1^{(Q)}(t-T_o-\tau_1)dt + T_w W_1^{(h)}(mT_w)\Big] \quad (2.24)$$

The second and the third terms in the square bracket are very small compared with the first and the fourth term values of T_w; therefore, the desired signal component can be approximated as follows:

$$x_{1,1}(m) \cong A_{1,1}(m)W_1^{(h)}(mT_w)\boldsymbol{a}(\theta_{1,1})$$

$$\cong \rho_1(m)\alpha_{1,1}(m)e^{-j\phi_{1,1}(m)}W_1^{(h)}(m)\boldsymbol{a}(\theta_{1,1}) \quad (2.25)$$

Equation (2.25) shows the expression for the desired signal used in the simulation. $\alpha_{1,1}(m)$ is the fading amplitude updated at every Walsh symbol, $\phi_{1,1}(m)$ is the phase changing from one Walsh symbol to the next due to channel fading, $\theta_{1,1}$ is the angle of arrival, and $\rho_1(m)$ is the power control parameter. The modeling of the power control parameter of the desired user will be presented in Section 2.2.4.

For the undesired signal component (i.e. $k \neq 1$ or $l \neq 1$), because of independent, identical and equiprobable distribution of PN chips among all user signals, we get:

$$\int_0^{T_o} c_k^{(I)}(t-t_l)c_l^{(I)}(t-T_o-t_l)dt = \pm T_o$$

$$\int_0^{T_o} c_k^{(Q)}(t-t_l)c_l^{(I)}(t-T_o-t_l)dt = \pm T_o$$

$$\int_0^{T_o} c_k^{(I)}(t-t_l)c_l^{(Q)}(t-T_o-t_l)dt = \pm T_o$$

$$\int_0^{T_o} c_k^{(Q)}(t-t_l)c_l^{(Q)}(t-T_o-t_l)dt = \pm T_o \qquad (2.26)$$

From equation (2.23), the undesired signal component can be expressed as follows:

$$x_{kl}(m) = A_{kl}(m)a(\theta_{kl})\frac{1}{2T_w}\left[\sum_{i=0}^{7}\pm T_c - j\sum_{i=0}^{15}\pm T_o + j\sum_{i=0}^{15}\pm T_o + \sum_{i=0}^{7}\pm T_c\right]$$

$$= A_{kl}(m)a(\theta_{kl})\left[\frac{1}{16T_c}\sum_{i=0}^{15}\pm T_c + j\frac{1}{32T_0}\sum_{i=0}^{31}\pm T_o\right]$$

$$= A_{kl}(m)a(\theta_{kl})\left[\frac{1}{16}\sum_{i=0}^{15}\pm a_i + j\frac{1}{32}\sum_{i=0}^{31}\pm a_i\right] \qquad (2.27)$$

where a_i is either 1 or -1 with equal probability. With the assumption of validity of equation (2.26), equation (2.27) is the expression for modeling the interference of each path. $A_{kl}(m)$ consists of the phase, the power control parameter, and fading amplitude of the interference for the k-th user and the l-th path. The method for modeling the power control parameter of each interfering user will be discussed in Section 2.2.4. The square bracket term is present in equation (2.27) because of non-zero correlation among users' PN sequences in the interval of every Walsh element. The interference consists of two binomial random variables in I-channel and Q-channel. In the simulation, instead of using

the binomial random variables, the interference of each path is modeled as two zero-mean Gaussian random variables in both in-phase and quadrature components separately. For 2.5MHz system, the variance of the in-phase interference for each path is 1/16; the variance of the quadrature interference - 1/32.

Therefore, the interference of each path can be added up individually in Walsh element by Walsh element form with its own phase, power control parameter, fading amplitude and angle of arrival. The pre-correlation signal vector of the 2.5MHz system for the first user and the first path is:

$$x(m) = \sum_{k=1}^{K}\sum_{l=1}^{L} x_{k,l}(m) = A_{1,1}(m)W_1^{(h)}(m)a(\theta_{1,1}) + i(m) + n(m) \qquad (2.28)$$

where $i(m)$ is the interference term containing the intersymbol and multiuser interference components, and $n(m)$ is due to the channel noise. It is noticed that only a single path desired signal exists in the 2.5MHz system and the other signals are interference.

Similarly, the pre-correlation signal vector for the 1.25MHz system, when the first user and the first path signal is perfectly tracked, is:

$$x(m) = A_{1,1}(m)W_1^{(h)}(m)a(\theta_{1,1}) + \frac{1}{2}A_{1,2}(m)W_1^{(h)}(m)a(\theta_{1,2}) + i(m) + n(m) \qquad (2.29)$$

It is noticed that a little piece of the desired second path signal is present in equation (2.29) because of the unresolvable path case (the time delay between the first and the second paths is one-half PN-chip period). Here, the variance of the in-phase interference for each path is 1/8; the variance of the quadrature interference - 1/16.

The pre-correlation signal vectors for the 1.25MHz and the 2.5MHz systems have been given in equations (2.28) and (2.29). The post-correlation signal vector $z(n)$ of the 2.5MHz system will be derived in the following. The post-correlation signal vector is the signal vector at the $\hat{h}$ -th output branch of the 64-ary Walsh sequence correlator.

$$z(n) = \sum_{m=0}^{64-1} x(n,m) W_r^{(h)}(n,m) \tag{2.30}$$

where $W_r^{(h)}(n,m)$ is the $\hat{h}$-th Walsh element sequence at the n-th Walsh symbol and the m-th Walsh element. If the estimated Walsh symbol value is wrong (i.e. $\hat{h} \neq h$), the desired signal components disappear in the post-correlation signal vector. Otherwise, the interference component in the post-correlation signal vector for the 2.5MHz system in baseband complex notation is:

$$z(n) = 64 A_{1,1}(n) a(\theta_{1,1}) + i'(n) + n'(n) \tag{2.31}$$

where $i'(n)$ is the interference term due to intersymbol and multiuser interference components and $n'(n)$ is due to the channel noise after Walsh sequence correlation. The interference is significantly reduced after the Walsh sequence correlation. This post-correlation signal vector will be used for explanation in Section 3.3.

2.2.4 Power control model

The section presents the modeling of the power control parameters for the desired user and each interfering user. We assume that the large-scale fading effects due to path loss and shadowing have been eliminated through the combined actions of open-loop and closed-loop power control. However, the IS-95 closed loop power control algorithm,

shown in Figure 2.3 and equations (2.32) to (2.34), is implemented to mitigate small-scale fading. A power control bit is transmitted by the base station to the mobile user every T_p ms requesting a fixed incremental change in the transmitted power. To generate the power control command bit, the received signal power is estimated from the 64-ary outputs of the IS-95 square-law combiner and compared with a threshold. This signal energy per Walsh symbol E_s is estimated by

$$E_s = \frac{1}{n_p}\sum_{n=1}^{n_p} z_{n,\hat{h}} - \frac{\bar{n}^2}{64-1} \quad . \tag{2.32}$$

$$z_{n,\hat{h}} = \max_f \left\{ z_{n,f} \right\} \tag{2.33}$$

$$\bar{n}^2 = \frac{1}{n_p}\sum_{n=1}^{n_p}\sum_{f=0, f\neq\hat{h}}^{64-1} z_{n,f} \tag{2.34}$$

where $\hat{h}$ is the estimated Walsh symbol value after the decision detector corresponding to the index of the largest decision value at the output of the IS-95 square-law combiner for the given Walsh symbol interval, $z_{n,f}$ is the f-th decision value at the output of the IS-95 square-law combiner at the n-th Walsh symbol interval. n_p is the number of Walsh symbols in the power control measurement interval of T_p ms. The estimated signal energy is then compared against a threshold and a power control bit is generated accordingly and sent to the mobile unit on the forward link to change the transmitted signal power of the mobile unit by a fixed increment. Here, the threshold is chosen so that the signal power per antenna is normalized to 1 [21]. The power control will not provide substantial reduction of required average SINR at a relatively high fading rate, while power control

can track channel variation better [22]. Due to the calculation delay and the transmission delay of a power control bit, the power control bit is activated in the mobile unit with a delay of a couple of T_p ms. In addition, because the power control bit is sent unprotected on the forward link, there is a probability of error in the received power control bit.

In this paper, the power control bit is updated at every sixth Walsh symbol with a power control step size of 1.0 dB. Each power control feedback bit is delayed with 12 Walsh symbol periods and suffers a 10% error rate.

The power-controlled multipath signal of each interfering user is modeled based on the statistical model of the power-controlled multipath signal of the desired user. After many runs of simulation, the average power $\bar{\mu}$ of the desired user and its standard derivation σ_s are calculated for different types of receivers as follows:

$$\bar{\mu} = E\left[10 \cdot \log\left[\sum_{l=1}^{L} A_{l,l}^2(n)\right]\right] \tag{2.35}$$

$$\sigma_s = \sqrt{E\left[\left[10 \cdot \log\left[\sum_{l=1}^{L} A_{l,l}^2(n)\right] - \bar{\mu}\right]^2\right]} \tag{2.36}$$

where E is the expected value of [ ]. The average power $\bar{\mu}$ is the ensemble average of the desired user's power-controlled multipath delay profile at every n-th Walsh symbol interval. The average power and its standard deviation are log-normal distributed and used to model the power-controlled multipath signal of each interfering user, mimicking the effect of the IS-95 power control algorithm on each interfering user.

2.3 Summary

In this chapter, the channel model, an IS-95 transmitter model, a single antenna receiver, an antenna array receiver and the closed-loop power control algorithm have been given. The expression for modeling the desired signal and interference have been derived in Walsh element forms. The interference of each path is modeled as Gaussian interference in both the I-channel and Q-channel with its own phase, angle of arrival, fading amplitude, and power control parameter.

3. ADAPTIVE ANTENNA ARRAYS

This chapter will explain the basic idea of the antenna array receiver, briefly discuss the array structure and the array geometry, and finally present different techniques for determining the complex weights of the spatial filter solution of the antenna array receiver.

3.1 Theory of a Uniform Linear Array

For clarity, to illustrate the basic idea of adaptive antenna array, we first consider a simple beamforming for a single-path channel case. The chosen array is linear with uniform half wavelength interelement separation. Figure 3.1 shows a simple beamformer with a uniform linear array.

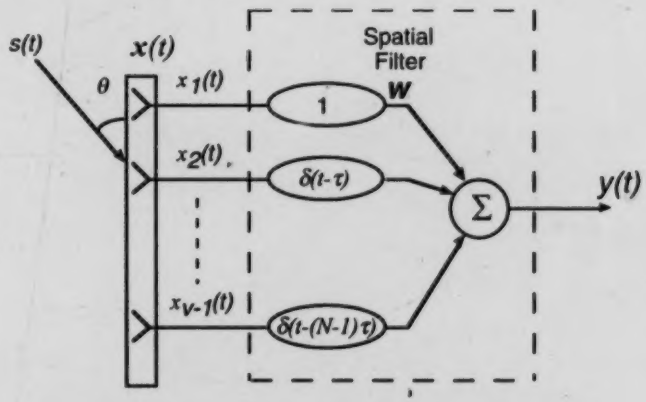

Figure 3.1. Diagram of a simple beamformer.

s(t) is a single narrowband signal received at the first array element with an azimuth angle of θ. Similar to the derivation of equation (2.17), the received signal vector *x(t)* is:

$$\boldsymbol{x}(t) = s(t)\boldsymbol{a}(\theta) + \boldsymbol{n}_o(t) \tag{3.1}$$

where $s(t)$ is a single narrowband signal, $n_o(t)$ is the channel noise vector, $a(\theta)$ is the array response vector. For a simple beamforming technique (without nulling operation), each array element output is co-phased by an appropriate phase shifter. A phase shift of Φ, called electrical angle, is inserted in the second array element, a phase shift of 2Φ in the third element, and a phase shift of $(v-1)\Phi$ in the v-th element. The electrical angle Φ is related to the electrical time delay τ as $\Phi = \omega_c \tau$ (time delay or time advance depends on the angle of arrival), where ω_c is the radian carrier frequency. So, the complex weights of the spatial filter solution w is simply a set of linear phase shifters to co-phase the array element outputs.

$$w = \frac{1}{\sqrt{V}}[1,\ exp(-j\Phi),\ldots,exp(-j(V-1)\Phi)]^T \tag{3.2}$$

Then, all co-phased array element outputs are summed up to obtain the weighted array output $y(t)$.

$$y(t) = w^H x(t) \tag{3.3}$$

where H is hermitian transpose. Because of the narrowband assumption, the complex envelope of the output $y(t)$ is:

$$Y(t) = S(t)\frac{1}{V}\sum_{v=0}^{V-1}\exp(-jv(\pi\cos\theta - \Phi)) + N(t) \tag{3.4}$$

where $S(t)$ is the complex envelope of the incoming narrowband signal $s(t)$, and $N(t)$ is the complex envelope of the total noise. When we adjust Φ to make it equal to $\pi cos\theta$, the signals received by array element from the direction θ are phase-synchronized and

coherently combined, but the noise is added incoherently. If the interfering signals are present in the environment, the interference from other directions is added incoherently. Hence, this array can enhance the desired signal from a particular direction and suppress the MAI from other directions in frequency reuse environment. Now, if we neglect the noise terms and replace $(\Phi - \pi\cos\theta)$ with $\pi\cos\theta$ (i.e. set the electrical angle Φ equal to zero), the equation (3.4) is reduced to:

$$Y(t) = S(t)\frac{1}{V}\sum_{v=0}^{V-1}\exp(-jv\pi\cos\theta) \tag{3.5}$$

The directional pattern of the array may be found by considering only the summation term in equation (3.5). It is called the array factor (that is, the relative sensitivity of array response to signals for a specific frequency from various directions):

$$F(\theta) = \frac{1}{V}\sum_{v=0}^{V-1}\exp(-jv\pi\cos\theta) \tag{3.6}$$

and the normalized directional antenna gain pattern is defined by

$$G(\theta) = |F(\theta)|^2 \tag{3.7}$$

Due to $\sum_{v=0}^{V-1} x^v = \frac{(x^v - 1)}{(x - 1)}$, the normalized directional gain pattern is:

$$G(\theta) = \left|\frac{1}{V}\sum_{v=0}^{V-1}\exp(-jv\pi\cos\theta)\right|^2 = \left[\frac{\sin\left(\frac{V\pi\cos\theta}{2}\right)}{V\sin\left(\frac{\pi\cos\theta}{2}\right)}\right]^2 \tag{3.8}$$

If we take the limit of the above expression, we get

$$\lim_{\theta \to 90^\circ} G(\theta) = \lim_{\theta \to 90^\circ} \left[\frac{\sin\left(\frac{V\pi \cos\theta}{2}\right) \Big/ \frac{V\pi \cos\theta}{2}}{V \sin\left(\frac{\pi \cos\theta}{2}\right) \Big/ \frac{V\pi \cos\theta}{2}} \right]^2 = 1 \qquad (3.9)$$

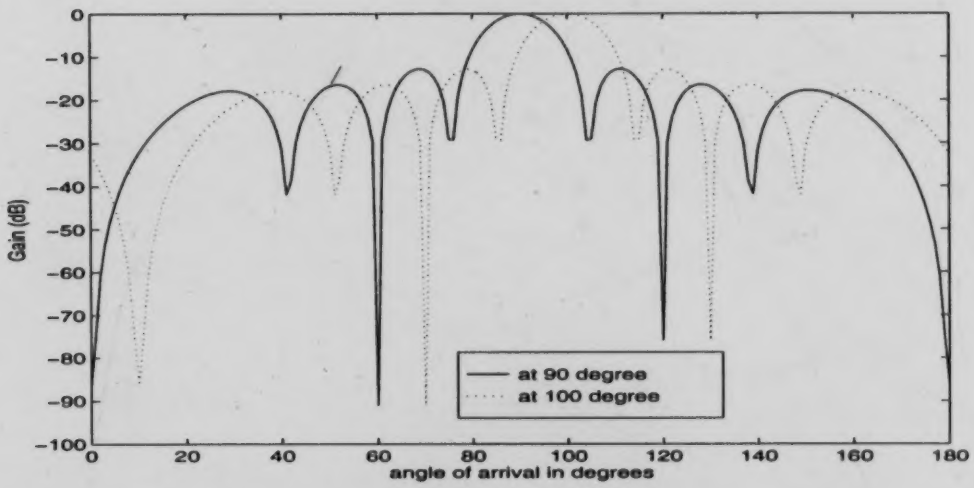

Figure 3.2. Normalized directional gain pattern for an eight-element uniform array.

$G(\theta)$ is plotted in Figure 3.2 for an eight element array steered along θ. The solid line is the mainlobe of the radiation pattern steered at $90°$ (i.e.$\Phi=0$); the dotted line - at $100°$. When we set $G(\theta) = 0$ to find the number of null points in the field of view, we discover the existence of $(V-1)$ null points. When the electrical angle Φ is zero (i.e. the solid-line pattern), the incoming signal arriving at $\theta = 90°$ is maximized because its wavefront is parallel to the array. If we set the numerator equal to zero, we can find the null points of the gain pattern.

$$\sin\left(\frac{V\pi\cos\theta}{2}\right)=0 \quad ,V\geq 2 \tag{3.10}$$

$$\frac{V\pi\cos\theta}{2}=i \quad ,i\in\{-\lfloor V/2\rfloor,\ldots,-1,1,\ldots,\lfloor V/2\rfloor\} \tag{3.11}$$

$$\theta=\cos^{-1}\left(\frac{2i}{V}\right) \tag{3.12}$$

where $\lfloor x \rfloor$ is the largest integer less than x for $x>0$ or the smallest integer larger than x for $x<0$. The mainlobe width (beamwidth) is $\cos^{-1}(-2/V) - \cos^{-1}(2/V)$ or $2(90° - \cos^{-1}(2/V))$. As V increases, the number of nulls increases. It is obvious that the beamwidth decreases as the number of array elements V increases [20].

For the adaptive antenna array, the weight factor τ is not a simple constant delay. Both the magnitude and the phase of the weights can be adapted independently to steer the mainlobe towards the direction of the desired signal and to place the nulls in the directions of the interfering signals.

3.2 Array Structure and Geometry

There are two kinds of adaptive antenna arrays: narrowband beamforming and wideband beamforming. The narrowband beamformer is used for processing narrowband signals, and it uses complex-valued weights in each branch of the combiner. In the wideband beamformer, each complex adaptive weight is replaced with a tapped-delay line (transversal filter) in order to process wideband signals. This replacement permits

frequency dependent amplitude and phase adjustments to be made [23-24]. Since the IS-95 system is a narrowband system, the narrowband beamforming is used in this thesis.

There are two types of array geometry: linear arrays and planar arrays. In a linear array the array elements are located along a straight line, while in a planar arrays all the array elements are located in one plane. The linear array can form a beam towards a specific azimuth angle.

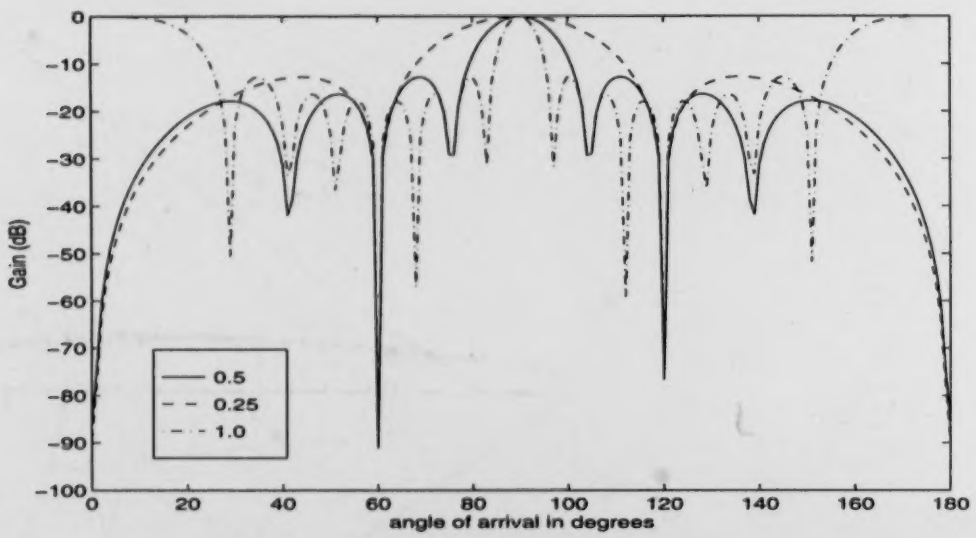

Figure 3.3. Radiation patterns formed by different values of interelement spacing.

Figure 3.3 shows the radiation patterns formed by a uniform linear array with different values of interelement spacing. The solid line denotes the interelement spacing of half-wavelength, the dash line - the spacing of quarter-wavelength, the dash-dotted line - the spacing of a wavelength. One principal lobe (or main beam) of the radiation pattern is produced when the array with half wavelength interelement separation is used. If the interelement separation is less than half wavelength, fewer nulls are created; if the

interelement separation is larger than half wavelength, the grating lobes which have an equal gain to the main lobe appear, because some array element signals are aligned exactly and add coherently at some specific directions. A planar array can form a conical beam pointing at some azimuth-elevation in space. A circular array, a type of planar array, is useful when angular symmetry is desired in a two-dimensional operation [24]. [25] shows that system capacity is highly dependent on the array geometry and orientation due to the highly non-uniform spatial distribution of users. In this thesis, a uniform linear array with half wavelength interelement spacing is chosen for further work.

3.3 Adaptive Antenna Array Techniques

There are different techniques to determine the complex weights of the spatial filter, from selecting the highest signal power of a fixed multiple beam network, through steering the mainlobe towards the desired signal, to both steering the mainlobe towards the desired signal and placing the nulls towards the interference. [8-9] show that the optimum combining techniques outperform the switched beam systems, simple beamformer, subspace-based techniques and the eigenfilter techniques.

3.3.1 Switched beam system

The switched beam system uses an antenna array in the base station to form multiple orthogonal fixed narrow beams covering the service area. The number of fixed beams is equal to the number of array elements. The array elements are connected together via a beamforming network (BFN). Each output of BFN corresponds to the

beam covering a given area and may receive desired signal components. The highest power output of the BFN is selected to pick out the desired signal. In the microcellular environment, the angular spread of the signal from a single user is very wide due to the low base station antenna and the close proximity of the scattering objects, so a few beam outputs which receive the desired multipath signal components arriving both within the same PN chip and at different PN chips can be combined non-coherently for further improvement.

The switched beam system might be considered as an extension of a conventional 3-sector cell sectorization to a narrow sector configuration. In the simple 3-sector cell sectorization, frequency assignment and hand-off are performed in the same manner as different cells when a mobile station moves over the different sectors in the same cell. The major difference is that the inter-sector hand-off is performed at the base station without signaling through the switch - the so called softer hand-off. Still a given amount of signaling between the base and mobile stations is required. The mechanism for processing hand-off puts restriction on the minimum sector size that can be implemented. Therefore, the advantage of the switched beam system is the elimination of inter-sector hand-off and thus narrower beam can be implemented [26].

3.3.2 Simple beamformer

The switched beam system selects the best beam from the multiple orthogonal fixed beams to receive the desired signal. The more effective approach is to use the simple beamformer to steer its main beam towards the desired signal. The simple beamformer uses the conventional beamformer (CBF) density spectrum to estimate the angle of arrival

of the desired signal. The CBF density spectrum displays an angular power density spectrum $P(\theta)$ along with the azimuth angle θ by the following equation.

$$P(\theta) = \boldsymbol{a}^H(\theta)\boldsymbol{R}\boldsymbol{a}(\theta) \tag{3.13}$$

where $\boldsymbol{R}$ is an auto-correlation matrix of a received array signal vector. The azimuth angle, producing the highest power of $P(\theta)$, is chosen to determine the electrical angle Φ to co-phase the array element outputs as discussed in Section 3.1. For the IS-95 systems, the post-correlation signal vector $z(n)$ in equation (2.31), instead of the pre-correlation signal vector $x(n)$ (the reason is the lower interference power in $z(n)$), is used in the conventional beamformer density spectrum.

$$P(\theta) = \boldsymbol{a}^H(\theta)\overline{\boldsymbol{R}}_{zz}\boldsymbol{a}(\theta) \tag{3.14}$$

$$\overline{\boldsymbol{R}}_{zz} = E\left[\boldsymbol{z}(n)\boldsymbol{z}^H(n)\right] \tag{3.15}$$

where E[ ] is the expected value. $\overline{\boldsymbol{R}}_{zz}$, called the ensemble-average of the post-correlation array covariance, is the ensemble-average of the auto-correlation matrix of the post-correlation signal vector (we can obtain $\overline{\boldsymbol{R}}_{zz}$ by averaging over a number of consecutive Walsh symbols). Because of the characteristics of PN chips among all user signals, the interference signal strength of each interfering path is significantly reduced in the post-correlation signal vector. The interference components are already much reduced in the matrix $\overline{\boldsymbol{R}}_{zz}$. From equations (2.31) and (3.15), the matrix $\overline{\boldsymbol{R}}_{zz}$, can be written in general form which is in terms of both the desired and interfering signal components of each path. The channel noise component is neglected.

$$\bar{R}_{zz} = \sum_{i=1}^{\ell} P_i a(\theta_i) a^H(\theta_i) + \sum_{i=\ell+1}^{I} P_i a(\theta_i) a^H(\theta_i) \quad , \; P_i > P_{i+1} \quad , \; P_\ell >> P_{\ell+i} \tag{3.16}$$

The first term is due to the desired signal component(s) and the second term is due to the interference of each path (here called the discrete interference), consisting of both the intersymbol and multi-user interference. P_i is the corresponding signal power with its own angle of arrival of θ_i, ℓ is the number of desired signal components, and $(I-\ell)$ is the total number of discrete interferers. $\ell = 1$ for the 2.5MHz system, while $\ell = 2$ for the 1.25MHz system. Equation (3.16) is obtained based on the following assumption:

$$E\left[a(\theta_i) a^H(\theta_g)\right] = 0, \quad i \neq g \tag{3.17}$$

Equation (3.17) implies that the array response vectors of two different paths are uncorrelated. When the main beam is steered towards the first desired signal component (i.e. $\theta=\theta_1$), from equations (3.14) and (3.16), the received power is:

$$P(\theta_1) = a^H(\theta_1)\left[\sum_{i=1}^{I} P_i a(\theta_i) a^H(\theta_i)\right] a(\theta_1)$$

$$= P_1 + \sum_{i=2}^{I} P_i a^H(\theta_1) a(\theta_i) a^H(\theta_i) a(\theta_1) \tag{3.18}$$

For a single desired signal component case, since $P_i << P_1$, $a^H(\theta_i)a(\theta_1) < 1$ and $a^H(\theta_1)a(\theta_1) = 1$, $P(\theta_1) \cong P_1$. The array response vector of the desired signal can be estimated by selecting the largest value of the conventional beamformer density spectrum $P(\theta)$. Equation (3.18) shows that $P(\theta_1)$ is composed of both the desired signal power and

the interfering signal power. Therefore, the distribution of the interference will degrade the array response vector estimation [8].

3.3.3 Subspace-based techniques

Subspace-based techniques use the eigen-decomposition to exploit the eigen-structure of the auto-correlation matrix of the received signal vector to better estimate the array response vector. There are a number of well-known high-resolution techniques such as MUSIC and ESPRIT [27-28]. Their detailed explanation can be found in [20]. Unfortunately, these algorithms works only if the number of array elements is greater than the number of signals. Although the number of user signals will by far exceed the number of array elements in mobile communication systems, the matrix $\overline{R}_{zz}$ of the IS-95 systems can be used for the eigen-decomposition analysis. The interference components are very small in the matrix $\overline{R}_{zz}$. Because of the assumption of the excellent characteristics of the PN codes and Gaussian approximation of all interference (i.e. the large number of users and a uniform distribution of angle of arrival of each interfering signal), the second term in equation (3.16) can be represented by Gaussian noise. This Gaussian noise is temporally and spatially white. Equation (3.16) becomes:

$$\overline{R}_{zz} = \sum_{i=1}^{\ell} P_i a(\theta_i) a^H(\theta_i) + \sigma^2 I$$

$$= \sum_{i=1}^{\ell} P_i a(\theta_i) a^H(\theta_i) + \sigma^2 \left[\sum_{i=1}^{\ell} e_i^s e_i^{s\,H} + \sum_{g=\ell+1}^{V} e_g^n e_g^{n\,H} \right] \quad , \quad P_i > P_{i+1} >> \sigma^2 \qquad (3.19)$$

where I is the identity matrix, σ^2 is the power of the Gaussian noise composed of both ISI and MAI, and V is the number of array elements. The number of e_i^s is ℓ; the number

of e_g^n - $(V-\ell)$. e_i^s and e_g^n are the orthonormal eigenvectors and form a unitary matrix U (one property of unitary matrix is $UU^H = I$):

$$U = [e_1^s, e_2^s, \ldots, e_\ell^s, e_{\ell+1}^n, \ldots, e_V^n] \tag{3.20}$$

When e_i^s is set equal to the array response vector of the i-th desired signal component (i.e. $e_i^s = a(\theta_i)$), e_i^s is called the i-th signal eigenvector, and thus e_g^n - the g-th noise eigenvector (the index g starts from $\ell+1$ to V). Equation (3.19) becomes:

$$\overline{R}_{zz} = \sum_{i=1}^{\ell} (P_i + \sigma^2) a(\theta_i) a^H(\theta_i) + \sigma^2 \sum_{g=\ell+1}^{V} e_g^n e_g^{nH} \tag{2.21}$$

Equation (3.21) can be written in the eigen-decomposition form:

$$\overline{R}_{zz} = U \Lambda U^H \tag{3.22}$$

$$\Lambda = diag[\lambda_1, \lambda_2, \ldots, \lambda_V] = diag[P_1 + \sigma^2, P_2 + \sigma^2, \ldots, P_\ell + \sigma^2, \sigma^2, \ldots, \sigma^2] \tag{3.23}$$

where ℓ is the number of the correlated signal components, P_i is the signal strength of the i-th desired signal component, λ_i is the eigenvalue, e_i^s and e_g^n in equation (3.20) are the signal and the noise eigenvectors associated with the corresponding eigenvalue in the diagonal matrix Λ. The noise eigenvectors e_g^n have the same eigenvalue σ^2. Since $\overline{R}_{zz} e_i^s = (P_i + \sigma^2) e_i^s$ and $\overline{R}_{zz} e_g^n = \sigma^2 e_g^n$, we have $e_i^{sH} \overline{R}_{zz} e_g^n = e_i^{sH} \sigma^2 e_g^n = \sigma^2 e_i^{sH} e_g^n$ and $e_i^{sH} \overline{R}_{zz} e_g^n = (\overline{R}_{zz} e_i^s)^H e_g^n = (P_i + \sigma^2) e_i^{sH} e_g^n$. Thus, $(P_i + \sigma^2) e_i^{sH} e_g^n = \sigma^2 e_i^{sH} e_g^n$ if and only if:

$$e_i^{s\,H} e_g^n = 0 \tag{3.24}$$

provided that $P_i + \sigma^2 \neq \sigma^2$. This orthogonality condition forms the cornerstone for the subspace-based algorithms. The signal eigenvectors form a signal space, while the noise eigenvectors - a null space which is used to determine the array response vector. Unlike simple beamformer, the subspace-based algorithm can clearly identify and distinguish the closely spaced multiple desired signal components as long as the number of array elements exceeds the number of desired signal components. However, if the number of array elements is less than the number of desired signal components, the eigen-decomposition is poorly defined and none of the noise eigenvectors exist.

In the urban wireless environment, multipath propagation with delays within a PN chip is quite common and the angular spread is wide due to the proximity of the scattering objects, so the subspace-based techniques performs poorly in the presence of the highly correlated multipath signals. [29] proposes a method to separate the multipath components within a chip duration. The switched beam system is used to generate orthogonal beams, and then the subspace-based techniques are used in a beam to provide a better array response vector estimation. The additional advantage is the reduction of the small-scale fading.

3.3.4 Eigenfilter techniques

The eigenfilter techniques directly estimate the dominant eigenvector corresponding to the largest eigenvalue of the matrix $\overline{R}_{zz}$ and then set the complex weights equal to the estimated dominant eigenvector. To find out the desired signal component in

$\overline{R}_{zz}$, the power method recursion [30-31], also called the power method, is the simplest iterative process to estimate the dominant eigenvector associated with maximum eigenvalue in the matrix $\overline{R}_{zz}$. The concept of the power method recursion is presented in the following.

The power method recursion solves the equation (3.25) by using the recursive iteration process given in equation (3.26):

$$A\hat{v} = \eta_{max}\hat{v} \tag{3.25}$$

$$v_{t+1} = \frac{Av_t}{\|Av_t\|} \tag{3.26}$$

$$\lim_{t\to\infty} v_t = \hat{v} \tag{3.27}$$

where A is a given matrix, $\hat{v}$ is the eigenvector corresponding to the dominant eigenvalue η_{max} of the matrix A, v_t is the estimated dominant eigenvector at the t-th iteration, and $\|\ \|$ is the vector norm. The power method recursion converges to $v_t = \hat{v}$ as $t\to\infty$. In practice, the number of iterations is not infinite. The termination criterion shown in equation (3.28) is used to determine how many iterations are required in equation (3.26).

$$\|v_{t+1} - v_t\| < \varepsilon \tag{3.28}$$

ε is the eigenvector estimation error. When the norm of the difference between the two subsequent estimated eigenvectors is less than ε, the iteration process is terminated and the estimated dominant eigenvector is found.

The following is the basic idea of the power method recursion. Let e_i be the eigenvector associated with the eigenvalue λ_i of the V-by-V matrix A. Any arbitrary $V \times 1$ vector v_0 can be written as:

$$v_0 = a_1 e_1 + a_2 e_2 + \cdots + a_t e_t + a_{t+1} e_{t+1} + \cdots + a_V e_V \quad , \quad a_1 \neq 0 \tag{3.29}$$

where a_i is a scalar. This vector is the initial vector for equation (3.26). If the initial vector does not contain a component of the dominant eigenvector (i.e. $a_1 = 0$), rounding error sustained during the iteration typically ensures that the subsequent v_t has a component of e_1. After t iterations, equation (3.26) becomes:

$$v_t = \gamma A^t v_0 = \gamma A^{t-1} A v_0 = \gamma A^{t-1} \left[a_1 A e_1 + a_2 A e_2 + \cdots + a_V A e_V \right] \tag{3.30}$$

where γ is a scalar due to the vector norm operation $\|Av_t\|$ in equation (3.26). Since $Ae_i = \lambda_i e_i$,,

$$\begin{aligned} v_t &= \gamma A^{t-1} \left[a_1 \lambda_1 e_1 + a_2 \lambda_2 e_2 + \cdots + a_V \lambda_V e_V \right] \\ &= \gamma \left[a_1 \lambda_1^t e_1 + a_2 \lambda_2^t e_2 + \cdots + a_V \lambda_V^t e_V \right] \\ &= \gamma a_1 \lambda_1^t \left[e_1 + \left(\frac{a_2}{a_1} \right) \left(\frac{\lambda_2}{\lambda_1} \right)^t e_2 + \cdots + \left(\frac{a_V}{a_1} \right) \left(\frac{\lambda_V}{\lambda_1} \right)^t e_V \right] \end{aligned} \tag{3.31}$$

Since $\lambda_1 > \lambda_2 > \cdots > \lambda_V$, $(\lambda_i / \lambda_1)^t << 1$ for $i \neq 1$ as t approaches to infinity or is sufficiently large (using termination criterion). Therefore, equation (3.31) becomes:

$$v_t = \gamma a_1 \lambda_1^t e_1 + \textit{neglected terms}, \quad t \to \infty \tag{3.32}$$

It is shown that power method recursion can be used to find the eigenvector associated with the dominant eigenvalue in the given matrix. Power method recursion converges quickly if the given matrix only contains one dominant eigenvalue and the initial vector v_0 has a component of the dominant eigenvector (i.e. $a_1 \neq 0$).

However, if $(\lambda_2/\lambda_1) \cong (\lambda_3/\lambda_1) \cong \cdots \cong (\lambda_\ell/\lambda_1) \cong 1$, the equation (3.31) becomes:

$$v_i \cong \gamma a_1 \lambda_1^i \left[e_1 + \left(\frac{a_2}{a_1}\right) e_2 + \cdots + \left(\frac{a_\ell}{a_1}\right) e_\ell \right] + \textit{neglected terms} \qquad (3.33)$$

The estimated dominant eigenvector contains ℓ eigenvectors

In the 2.5MHz system, the base station receives a single desired signal component and many interference component. A single dominant eigenvalue associated with the desired signal component exists in the matrix $\overline{R}_{zz}$, and the rest of eigenvalues are very small. The estimated eigenvector, estimated by power method recursion under an appropriate value of the eigenvector estimation error, is the array response vector of the single desired signal. When the complex weights of the spatial filter are set equal to the estimated eigenvector, the mainlobe is steered towards the desired signal. However, in the 1.25 MHz system, two desired signal components may arrive at the base station with relatively equal signal strength, the estimated dominant eigenvector consists of the array response vectors of the two desired signal components. When the complex weight vector is set equal to the estimated combined vector, a mainlobe and a sidelobe are steered towards the two desired signal components.

3.3.5 Optimum combining techniques

The above approaches attempt to maximize the signal power by steering the mainlobe and sidelobes towards the desired signals. These approaches are optimal and maximize the SINR when the interference is spatially and temporally white. However, if the CDMA interference does not follow this distribution, the performance loss will result. Therefore, optimum combining techniques are used to maximize the SINR by placing nulls towards the interference and steering main beam and sidelobe(s) towards the desired signal(s). Both the magnitude and the phase of each complex weight can be adjusted to achieve the optimum spatial filter solution. Theoretically, the maximum number of interference signals that an array can suppress is equal to one less than the number of elements in the antenna array. In the urban wireless environment, the number of interfering signal components is by far larger than the number of array elements, so the capability of interference suppression in that system is still not optimal. The optimum combining techniques are governed by the minimum mean-square-error criterion and thus minimize the squared difference of the desired data sequence and the weighted array output. The cost function ξ is written as follows:

$$\begin{aligned}\xi &= \mathrm{E}\left[\left|d(n) - w^H z(n)\right|^2\right] \\ &= \mathrm{E}\left[d^2(n)\right] - 2w^H \mathrm{E}\left[z(n)d(n)\right] - w^H \mathrm{E}\left[z(n)z^H(n)\right]w \\ &= \mathrm{E}\left[d^2(n)\right] - 2w^H \Phi - w^H \overline{R}_{zz} w \end{aligned} \tag{3.34}$$

$$\overline{\Phi} = \mathrm{E}[z(n)d(n)] \tag{3.35}$$

where $d(n)$ is the desired data sequence, and $\overline{\Phi}$ is the ensemble average of the product of the post-correlation signal vector and the desired data sequence. This vector $\overline{\Phi}$ is here called the ensemble-average product vector. This function is a quadratic function and the optimum spatial filter solution w can be obtained by setting the derivative of (3.34) with respect to w to zero.

$$\frac{d}{dw}\xi = 2\overline{\Phi} - 2\overline{R}_{zz}w = 0 \tag{3.36}$$

$$w = \overline{R}_{zz}^{-1}\,\overline{\Phi} \tag{3.37}$$

This optimum spatial filter solution is called the Wiener filter solution. The main difficulty here is to determine the desired data sequence. It is possible to employ periodic training sequences to determine the spatial filter solution, but this approach reduces the efficiency of the reverse link transmissions. Another approach is to use the previous decision of the complex weights to estimate the current desired data sequence; this is called the feedback-previous-decision approach. Performance losses inherently result because of the wrong estimates of the desired data sequence.

The other spatial filter solution which can achieve the same Wiener filter solution in equation (3.37) is shown in the following.

$$w = \overline{R}_{nn}^{-1}a \tag{3.38}$$

where $\overline{R}_{nn}^{-1}$ is the inverse of the ensemble-average array interference covariance matrix which contains no desired signal components. a is the vector composed of the array response vectors of the desired signal components. The idea is that a in equation (3.38)

steers the mainlobe and sidelobe(s) of the radiation pattern towards the desired signals and $\overline{R}_{nn}^{-1}$ in equation (3.38) directs the nulls at the interference. The proof of the equivalence of equations (3.37) and (3.38) is presented in the following.

When a single signal component is present in the received signal (i.e. the 2.5MHz system), equation (3.16) can be written as:

$$\overline{R}_{zz} = P_1 a(\theta_1) a^H(\theta_1) + \overline{R}_{nn} \quad , \qquad P_1 >> P_{i+1} \tag{3.39}$$

$$\overline{R}_{nn} = \sum_{i=2}^{I} P_i a(\theta_i) a^H(\theta_i) \tag{3.40}$$

where $\overline{R}_{nn}$ is the ensemble-average array interference covariance matrix, consisting ISI and MAI. The ensemble-average cross-product vector is $\overline{\Phi} = \sqrt{P_1}\, a(\theta_1)$. Substituting equation (3.40) into equation (3.37), one obtains

$$w = \left[P_1 a(\theta_1) a^H(\theta_1) + \overline{R}_{nn} \right]^{-1} \sqrt{P_1}\, a(\theta_1) \tag{3.41}$$

Applying the matrix inversion identity to equation (3.41), one gets

$$\left[P^{-1} + M^H Q^{-1} M \right]^{-1} \equiv P - PM^H \left[MPM^H + Q \right]^{-1} MP \tag{3.42}$$

The spatial filter solution becomes:

$$w = \sqrt{P_1} \left[\overline{R}_{nn}^{-1} - \frac{P_1 \overline{R}_{nn}^{-1} a(\theta_1) a^H(\theta_1) \overline{R}_{nn}^{-1}}{1 + P_1 a^H(\theta_1) \overline{R}_{nn}^{-1} a(\theta_1)} \right] a(\theta_1)$$

$$= c \overline{R}_{nn}^{-1} a(\theta_1) \tag{3.43}$$

$$\varsigma = \frac{\sqrt{P_l}}{1 + P_l a^H(\theta_l)\bar{R}_{nn}^{-1} a(\theta_l)} \tag{3.44}$$

where ς is a scalar. It is shown that equation (3.37) is related to equation (3.38) only by a scalar gain factor, and hence equation (3.38) represents the Wiener filter solution [24]. [17] shows that RLS is a suitable algorithm for equation (3.37) in the urban wireless channel because of the fast rate of convergence. [18] implements equation (3.38) in the IS-95 system by using the power method recursion for array response vector estimation; the algorithm is called recursive adaptive beamforming. In this paper, both spatial filter solutions in (3.37) and (3.38) are implemented. The RLS algorithm, having a Wiener filter solution of equation (3.37), is implemented in Walsh element form. For the second spatial filter solution in equation (3.38), two modified forms of the recursive adaptive beamforming are implemented. All three algorithms uses the feedback-previous-decision approach to determine the current transmitted Walsh symbol value in the IS-95 CDMA systems.

3.4 Summary

In this chapter, the basic idea of how an antenna array works in the receiver has been explained in detail. Then, antenna array structure and geometry have been analyzed and thus narrowband beamforming using a uniform linear array with half wavelength interelement distance is chosen for further study. Several techniques have been presented for the narrowband uniform linear antenna array receivers. Switched beam network selects

a fixed beam with the highest signal power from a multiple beam network. Simple beamformer steers the mainlobe towards the direction producing the highest power; the spatial filter solution is simply a set of the phase shifters. The subspace-based techniques can provide more accurate estimate of the angles of arrival of the desired signals. The eigenfilter techniques can steer mainlobe and sidelobes towards the desired signals. However, all the above methods do not null the interference. The optimal combining techniques can adapt both the magnitude and the phase of the complex weights so that the mainlobe and sidelobes are directed towards the desired signals and the nulls are placed at the interference. The recursive least squares algorithm and two modified forms of recursive adaptive beamforming can achieve optimum spatial filter solution in the time-varying channel and will be presented in more detail in the next chapter.

4. ADAPTIVE ANTENNA ARRAY ALGORITHMS

In this chapter, an antenna array for the current IS-95 system is proposed. The recursive least squares algorithm and two modified forms of recursive adaptive beamforming algorithms are discussed in detail.

4.1 IS-95 Antenna Array Structure

The idea of an adaptive antenna array reception is to use several highly correlated outputs of antenna array elements and the complex weights of the spatial filter to form beams toward the desired signals and nulls toward the interference. The RLS algorithm [17] and two modified forms of the RAB algorithm [18] are used to recursively adapt the complex weights of the IS-95 antenna array system. The uplink is simulated on a chip by chip basis in [17-18], using PN chip; on the other hand, it is simulated on an element by element basis in this thesis, using Walsh element. Therefore, the pre-correlation signal vector is the signal vector before PN-despreading in [18], but it is the signal vector before Walsh sequence correlation in this thesis. Every Walsh element is spread by 4 PN chips in the 1.25MHz system. The structure of the linear antenna array used to illustrate the RLS and two modified forms of the RAB algorithm in the IS-95 system is shown in Figure 4.1.

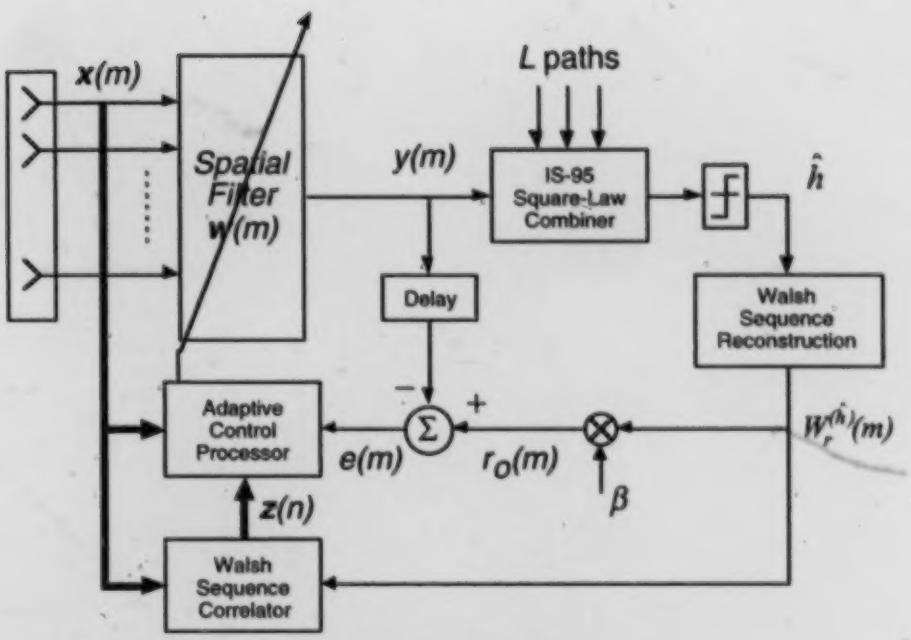

Figure 4.1. Linear adaptive antenna array structure.

We have considered a two-dimensional RAKE receiver for the antenna array. In one dimension of the two-dimensional RAKE involves coherent combining of the array element outputs through a so called spatial filter $w(m)$. The RLS algorithm updates the complex weights Walsh element by Walsh element (i.e. in terms of m-th Walsh element), while the RAB algorithms are updated Walsh symbol by Walsh symbol (i.e. in terms of n-th Walsh symbol). The complex weights of the spatial filter are adapted by a chosen adaptive control processor. The other dimension involves L-path noncoherent combining of all the outputs of the spatial filters in the IS-95 square-law combiner as described in Figure 2.3; this is the multipath noncoherent RAKE combining. The number of the spatial filters is determined by the number of temporal RAKE fingers, and the complex weights of each spatial filter are adapted independently.

The feedback-previous-decision approach is used to estimate the transmitted Walsh symbol h in all three algorithms. The weighted array output, $y(m) = \mathbf{w}^H (m-1)\mathbf{x}(m)$, is the dot product of the previous complex weight vector and the pre-correlation signal vector. Then, the weighted array output is fed into the IS-95-type square-law combiner shown in Figure 2.3, which performs L-path noncoherent combining. The estimated Walsh symbol value $\hat{h}$ is then obtained to reconstruct the estimated Walsh element sequence $W_r^{(h)}(m)$.

For the RLS algorithm, both the pre-correlation signal vector and the error signal $e(m)$ are required for adaptation. The error signal, $e(m) = r_o(m) - y(m)$, is the difference between a reference signal and the weighted array output. The reference signal, $r_o(m) = \beta W_r^{(h)}(m)$, is equal to the reconstructed Walsh element sequence $W_r^{(h)}(m)$ multiplied by the constant β, called here the reference signal magnitude. The complex weights are recursively updated over 64 iterations (each Walsh element is updated for one iteration), and then the final complex weight vector is normalized to 1 and used to obtain a better estimate of h.

For the two modified forms of RAB algorithms, both the pre-correlation signal vector and the post-correlation signal vector are required. The post-correlation signal vector is generated by correlating the pre-correlation signal vector and the reconstructed Walsh element sequence $W_r^{(h)}(m)$. After adaptation for each Walsh symbol, the new complex weights are normalized to 1 and then used to obtain a better estimate of h.

Since the wrong estimate of h will result in performance losses in the feedback-previous-decision approach and the recently estimated Walsh symbols may be wrong in a deep fade, the channel information obtained from the adequate number of the previous Walsh symbols must be used to provide a better estimate of the current Walsh symbol. Thus, the matrix time updates with an appropriate value of the forgetting factor are used to implement the RLS and the two modified forms of RAB algorithms.

4.2 Recursive Least Squares Algorithm

The RLS algorithm makes the adaptive array to form a main beam and sidelobes in the directions of the desired multipath signals while forming nulls in the directions of the interference automatically without the knowledge of the directions of the desired signal and interference. This algorithm adjusts the complex weights Walsh element by Walsh element to minimize the mean square value of the error signal *e(m)* (minimum mean square error criterion). If β is chosen so that the reference signal closely approximates that portion of the array output due to the desired signal, the error signal will mainly contain the undesired components of the array output. Minimizing the error signal corresponds to minimizing the antenna response to these undesired signals and results in a pattern of nulls in the directions of the interfering signals [32]. The detailed derivation can be found in [33]. Since the RLS algorithm adapts the complex weights Walsh element by Walsh element (RAB algorithms - Walsh symbol by Walsh symbol), the time-updated version of

the cost function $\xi(m)$ with exponential weighting, also called the forgetting factor, is shown in equation (4.1).

$$\xi(m) = \sum_{i=1}^{m} \mu^{m-i} \left| r_o(i) - w^H(m)x(i) \right|^2 \tag{4.1}$$

where the forgetting factor μ is a real positive constant close to, but less than, 1. Similar to the derivation from (3.34) to (3.37), the spatial filter solution of the RLS algorithm is:

$$w(m) = R_{xx}^{-1}(m)\, \Phi(m) \tag{4.2}$$

$$R_{xx}(m) = \sum_{i=1}^{m} \mu^{m-i} x(i)x^H(i) \tag{4.3}$$

$$\Phi(m) = \sum_{i=1}^{m} \mu^{m-i} x(i)W_r^{(k)}(i)^* \tag{4.4}$$

where $R_{xx}(m)$ is the V-by-V time-updated version of the auto-correlation matrix of the pre-correlation signal vector $x(m)$, $\Phi(m)$ is the V-by-1 time-updated version of the ensemble-average product vector $\overline{\Phi}$. * denotes complex conjugate. Both (4.3) and (4.4) can be recursively updated as follows:

$$R_{xx}(m) = \mu R_{xx}(m-1) + x(m)x^H(m) \tag{4.5}$$

$$\Phi(m) = \mu \Phi(m-1) + x(m)d^*(m) \tag{4.6}$$

Consequently, the inverse of $R_{xx}(m)$ is obtained by the use of a form of the *matrix inversion lemma* [33]:

$$B^{-1}(n) = \frac{1}{\mu}\left[B^{-1}(n-1) - \frac{B^{-1}(n-1)pp^H B^{-1}(n-1)}{\mu + p^H B^{-1}(n-1)p} \right] \tag{4.7}$$

where $B(n)$ is an $V \times V$ positive-definite matrix and p is a $V \times 1$ vector. $B(n)$ is defined as $B(n) = \mu B(n-1) + pp^H$. Hence,

$$R_{xx}^{-1}(m) = \frac{1}{\mu}\left[R_{xx}^{-1}(m-1) - \frac{R_{xx}^{-1}(m-1)x(m)x^H(m)R_{xx}^{-1}(m-1)}{\mu + x^H(m)R_{xx}^{-1}(m-1)x(m)}\right] \tag{4.8}$$

For simplicity, the procedure $B^{-1}(n)$=Inverse_update($B^{-1}(n-1)$, p, μ) implements equation (4.7). From equations (4.2), (4.6) and (4.8), the complex weight vector is:

$$w(m) = w(m-1) + K(m)e^*(m) \tag{4.9}$$

where $K(m)$ is the Kalman gain vector, defined as

$$K(m) = R_{xx}^{-1}(m)x(m) = \frac{R_{xx}^{-1}(m-1)x(m)}{\mu + x^H(m)R_{xx}^{-1}(m-1)x(m)} \tag{4.10}$$

and $e(m)$ is the error signal obtained by the previous complex weight vector.

$$e(m) = r_o(m) - w^H(m-1)x(m) \tag{4.11}$$

To apply the RLS algorithm, it is first required to initialize the inverse of the matrix $R_{xx}^{-1}(0)$. A simple procedure involves the following assignment.

$$R_{xx}^{-1}(0) = \delta_o^{-1} I \tag{4.12}$$

where I is an identity matrix and δ_o is a small positive constant such as 1.0. The elements of the initial complex weight vector are set to zero. The RLS algorithm can be summarized as follows:

RLS algorithm [33]

A. Initialize the RLS algorithm by setting

$$R_{xx}^{-1}(0) = \delta_o^{-1} I$$

$$w(0) = 0$$

B. For each instant of time, $m = 1, 2, \ldots$, compute

1. $e(m) = r_o(m) - w^H(m-1)x(m)$

2. $$w(m) = w(m-1) + \frac{R_{xx}^{-1}(m-1)x(m)}{\mu + x^H(m)R_{xx}^{-1}(m-1)x(m)} e^*(m)$$

3. $$R_{xx}^{-1}(m) = \frac{1}{\mu}\left[R_{xx}^{-1}(m-1) - \frac{R_{xx}^{-1}(m-1)x(m)x^H(m)R_{xx}^{-1}(m-1)}{\mu + x^H(m)R_{xx}^{-1}(m-1)x(m)} \right]$$

C. If $m = 63$, then $w(63) = \dfrac{w(63)}{\|w(63)\|}$

where $R_{xx}^{-1}(m)$ is the updated autocorrelation matrix of the pre-correlation signal vector $x(m)$. $e(m)$ is the error signal, I is an identity matrix, δ_o is a small positive constant such as 1.0, and μ is the forgetting factor which is very dependent on the fading rate of the channel with the best value close to 1. * denotes complex conjugate and H - Hermitian transpose. This algorithm will recursively adapt the complex weight vector to the Wiener filter solution.

Since the reference signal magnitude β is assigned a fixed real value, the error signal will contain the desired component of the array output and the phase of the desired signal. The RLS algorithm tries to shape the weighted array output to match the real-valued reference signal. If the phase of the desired signal varies, the degradation of the

RLS performance will occur. Therefore, RLS algorithm is phase-dependent and requires precise phase tracking.

4.3 Two Modified Recursive Adaptive Beamforming Algorithms

Due to the inaccuracy of the Walsh symbol estimates and the characteristic of the time-varying channel, the matrix time-update technique is used to implement equation (3.38). Both RAB(a) and RAB(b) algorithms adapt the complex weights Walsh symbol by Walsh symbol. The spatial filter solution of the RAB algorithm is given as follows:

$$w(n) = \hat{Q}^{-1}(n)\hat{a}(n) \tag{4.13}$$

where $\hat{Q}^{-1}(n)$ is the inverse of the estimated array interference covariance matrix at the n-th Walsh symbol and $\hat{a}(n)$ is the estimated array response vector of the desired signal. The estimated array interference covariance matrix ideally contains no component of the desired signal. Now, let's consider the 2.5MHz system. From equation (2.28), the pre-correlation signal vector $x(n,m)$ at the n-th Walsh symbol and at the m-th Walsh element is:

$$x(n,m) = A_{1,1}(n,m)W_1^{(h)}(n,m)a(\theta_{1,1}) + i(n,m) + n(n,m) \tag{4.14}$$

The pre-correlation array covariance matrix $R_{xx}(n)$ at the n-th Walsh symbol is defined by:

$$R_{xx}(n) = \sum_{m=0}^{64-1} x(n,m)x^H(n,m) = 64A_{1,1}^2(n)a(\theta_{1,1})a^H(\theta_{1,1}) + Q_{xx}(n) \tag{4.15}$$

where $Q_{xx}(n)$ is the array interference covariance matrix in the pre-correlation array covariance matrix due to the self-interference, multiple access interference and noise. From equation (2.22) we obtain:

$$A_{1,1}^2(n) = \rho_1^2(n)\alpha_{1,1}^2(n) \tag{4.16}$$

$A_{1,1}^2(n)$ does not depend on the phase of the desired signal, and hence, equation (4.15) does not contain the phase of the desired signal. From (2.31), the post-correlation signal vector $z(n)$ at the n-th Walsh symbol is:

$$z(n) = 64A_{1,1}(n)a(\theta_{1,1}) + i'(n) + n'(n) \tag{4.17}$$

The post-correlation array covariance matrix $R_{zz}(n)$ is:

$$R_{zz}(n) = z(n)z^H(n) = 64^2 A_{1,1}^2(n)a(\theta_{1,1})a^H(\theta_{1,1}) + Q_{zz}(n) \tag{4.18}$$

where $Q_{zz}(n)$ is the array interference covariance matrix in the post-correlation array covariance matrix due to the self-interference, multiple access interference and noise. The equation (4.18) does not contain the phase of the desired signal. We assume:

$$Q_{xx}(n) = Q_{zz}(n) = Q(n) \tag{4.19}$$

where $Q(n)$ is the array interference covariance matrix.

Now, the first step is to estimate the inverse of the estimated array interference covariance matrix $\hat{Q}^{-1}(n)$ in equation (4.13). Manipulation of equations (4.15), (4.18) and (4.19) yields the array interference covariance matrix:

$$Q(n) = \frac{64}{(64-1)}\left[\sum_{m=0}^{64-1} x(n,m)x^{H}(n,m) - \frac{1}{64} z(n)z^{H}(n)\right] \tag{4.20}$$

The estimated array interference covariance matrix $\hat{Q}(n)$ is the time update version of the array interference covariance matrix obtained from equation (4.20) can be:

$$\hat{Q}(n) = \mu\hat{Q}(n-1) + \frac{64}{(64-1)}\left[\sum_{m=0}^{64-1} x(n,m)x^{H}(n,m) - \frac{1}{64} z(n)z^{H}(n)\right] \tag{4.21}$$

where μ is the forgetting factor. The matrix inversion lemma in equation (4.7) is used to find the inverse of the estimated array interference covariance matrix $\hat{Q}^{-1}(n)$.

The second step is to find the estimated array response vector of the desired signal $\hat{a}(n)$ in equation (4.13). As mentioned in Section 3.3.4., the power method recursion in equation (3.26), working with the termination criterion in equation (3.28), is the simplest iterative process to estimate the dominant eigenvector associated with the maximum eigenvalue in the given matrix. If there is more than one dominant eigenvalue in the matrix, the estimated vector is the combined vector containing the dominant eigenvectors associated with their relatively equal eigenvalues. In the 2.5MHz system, the receiver receive a single desired signal, and thus a single desired signal component exists in both matrices $R_{xx}(n)$ and $R_{zz}(n)$ with the highest signal strength. On the other hand, the 1.25MHz system receiver may receive the first and the second desired signals in the first RAKE finger with relatively equal strength, and thus two corresponding highest eigenvalues exist in both matrices. The power method recursion will estimate the

combined vector containing the two array response vectors of the desired signals. Let us use the 2.5MHz system receiver to illustrate the two modified forms of RAB algorithms.

There are two different approaches, RAB(a) and RAB(b), for estimating the array response vector $a(\theta_{1,1})$. The first approach, called RAB(a), finds the dominant eigenvector of the time-updates of the matrix $R_{zz}(n) - R_{xx}(n)$, obtained from (4.15), (4.18) and (4.19).

$$A(n) = \mu A(n-1) + \left[R_{zz}(n) - R_{xx}(n)\right] \tag{4.22}$$

$$R_{zz}(n) - R_{xx}(n) = z(n)z^H(n) - \sum_{m=0}^{64-1} x(n,m)x^H(n,m) = (64^2 - 64)A_{1,1}^2(n)a(\theta_{1,1})a^H(\theta_{1,1}) \tag{4.23}$$

The estimated array response vector $\hat{a}(n)$ is equal to the eigenvector $a(\theta_{1,1})$ corresponding to the dominant eigenvalue of the matrix $R_{zz}(n) - R_{xx}(n)$, which ideally contains no desired signal components. The power method recursion is used to determine the eigenvector of the matrix given by equation (4.22). The other approach, called RAB(b), uses $R_{zz}(n)$ to determine the estimate of $a(\theta_{1,1})$.

$$A(n) = \mu A(n-1) + R_{zz}(n) \tag{4.24}$$

$$R_{zz}(n) = z(n)z^H(n) = 64^2 A_{1,1}^2(n)a(\theta_{1,1})a^H(\theta_{1,1}) + Q_{zz}(n) \tag{4.25}$$

The dominant eigenvalue in $R_{zz}(n)$ corresponds to an eigenvector of $R_{zz}(n)$ which is equal to the array response veetor $a(\theta_{1,1})$ of the desired signal. RAB(b) provides quite accurate array response vector estimate because the interfering signals' strength in $Q_{zz}(n)$ is already reduced significantly.

The purpose of using the time updates of the matrices in equations (4.22) and (4.24) is to provide more stable array response vector estimation by considering a longer received signal. In the above derivation, the phase of the desired signal is canceled out in the vector multiplication, so both RAB(a) and RAB(b), unlike the RLS algorithm, are phase-independent. They work properly and have similar performance in both the unknown and known phase environments. The two modified forms of RAB algorithms, RAB(a) and RAB(b), are implemented as follows:

RAB(a) and RAB(b) algorithms

1. Initialize the RAB(a) or RAB(b) algorithm by setting

$$A(0) = \delta_0^{-1} I$$

$$\hat{Q}^{-1}(0) = \delta_0^{-1} I$$

$$\hat{a}(0) = 0.1$$

$$w(0) = 0$$

2. For each instant of time, n=1,2,..., compute

1. $B^{-1}(0)$ = Inverse_update($\hat{Q}^{-1}(n-1), a\,x(n,0), \mu$)

2. For m = 1,2,...,63

$B^{-1}(m)$ = Inverse_update($B^{-1}(m-1), a\,x(n,m)$, 1)

3. $\hat{Q}^{-1}(n)$ = Inverse_update($B^{-1}(63), b\,z(n)$, 1)

4. if RAB(a)

$$A(n) = \mu A(n-1) + z(n)z^H(n) - \sum_{m=0}^{64-1} x(n,m)x^H(n,m)$$

else if RAB(b)

$$A(n) = \mu A(n-1) + z(n)z^H(n)$$

5. $v_0(n) = \hat{a}(n-1)$

6. (a) $v_{t+1}(n) = A(n)v_t(n) / \|A(n)v_t(n)\|$

(b) if $\|v_{t+1}(n) - v_t(n)\| < \varepsilon$

then $\hat{a}(n) = v_{t+1}(n)$, go to (c)

else $t \Rightarrow t+1$, go to (a)

(c) $w(n) = \hat{Q}^{-1}(n)\hat{a}(n)$

7. $w(n) \Leftarrow w(n) / \|w(n)\|$

where $a = \sqrt{64/(64-1)}$, $b = \sqrt{-1/(64-1)}$ and δ_o=1. μ is the forgetting factor and ε is the eigenvector estimation tolerance. From step(1) to step (3), the procedure $K^{-1}(n)$=Inverse_update($K^{-1}(n-1), p, \mu$) performs the recursive time-updating, where K is a $V \times V$ positive-definite matrix and p is a $V \times 1$ vector. The estimated array interference covariance matrix is calculated from step (1) to step (3). Step (4) determines whether RAB(a) or RAB(b) is used. Steps (5) and (6) implement the power method recursion and calculate the complex weight vector. Finally, step (7) normalizes the complex weight vector.

4.4 Summary

In this section, the application of the adaptive antenna array in the current IS-95 system is considered. The derivation of the recursive least squares algorithm and two modified forms of recursive adaptive beamforming are also presented. The RLS is a phase-dependent algorithm, which requires precise phase tracking mechanism, while both RAB(a) and RAB(b) are phase-independent.

5. SIMULATIONS AND RESULTS

For complex systems such as wireless communication systems, performance analysis using pure analytical means can be extremely difficult and abstract. Therefore, computer simulation, a relatively simple process, has become indispensable to evaluate the performance of complex systems. This chapter is concerned with the performance evaluation in the IS-95 reverse link by computer simulation of a single antenna, a dual-antenna and an adaptive antenna receiver discussed in previous chapters. Those receivers are simulated in a single cell microcellular environment with 100% voice activity at fading rates of 10Hz and 100Hz, and within both the 1.25MHz and the 2.5MHz systems. A linear antenna array containing eight elements with half wavelength separation has been assumed. For the RAKE reception case, two fingers of the RAKE are used to perfectly track the first path and the third path signals in the 1.25MHz system, while four fingers are used to capture four paths in the 2.5MHz system.

In the 1.25MHz system, each Walsh element is spread by 4 PN chips, while in the 2.5MHz system it is spread by 8 PN chips. Because of the independent, identical and equiprobable distribution of PN chips among all user signals, we only need to run the simulation Walsh element by Walsh element (and not chip-by-chip). The interference of each path is modeled as Gaussian in both the I-channel and the Q-channel, with its own angle of arrival, phase and independent fading amplitude. The envelope of the first path signal follows the Ricean fading, and the other paths follow the Rayleigh fading. The angle of arrival of each path is fixed over each simulation (about 50 frames) and the phase of

each path changes from one Walsh symbol to the next due to channel fading. The phase varies corresponding to the speed of mobile (i.e. 0.8° phase change for adjacent Walsh symbols in 10Hz fading rate case and 8° - in 100Hz case). The self-interference and the channel noise are neglected in the simulation.

5.1 Simulation Methodology

A commonly used performance measure for a digital communication system is its average bit error rate (BER). In this project, Monte Carlo simulation [34] is used to estimate the BER. This method requires no assumptions about the input process or the system and only compares the known input data sequence with the estimated output data sequence to obtain the estimated BER. In this chapter, the input data sequence is the 9.6 kbps data stream; the output data sequence is the 1/3-convolutionally decoded bit sequence. We count the number of errors in the bit sequence and divide it by the number of observed bits. The number of the observed bits must be large enough to obtain the estimated BER within acceptable confidence interval. If one hundred bit errors are counted, the estimated BER is within 25% of the actual BER 95% of the time. Each frame consists of 184 input data bits, excluding 8 appended zero bits. If 50 runs and 50 frames in each run are simulated, 460 error bits will be counted to produce quite accurately estimated 0.1% BER. 50 frames in each run, equivalent to 1 second observation time, encounter a few -40 dB deep fades at the fading rate of 100Hz (see Figure 1.3), which implies that the length of the observation interval is sufficient to estimate the BER reliably. The power control algorithm is not able to significantly mitigate fades at the

100Hz rate; on the other hand, it can effectively eliminate much less frequent -40 dB deep fades at the 10Hz fading rate. Therefore, 50 frames observation interval for each run is long enough to estimate 0.1% BER in both cases.

The expressions for modeling the desired signal and interference are given in equations (2.27), (2.28), and (2.29). The desired signal is power-controlled using the power control algorithm in equations (2.32), (2.33) and (2.34). The first power control bit of the desired user is issued at the 6-th elapsed Walsh symbol and activated after the additional delay of 12 Walsh symbols; this approach is taken to simulate the behavior of the IS-95 link as closely as possible. In order to simulate the effect of the IS-95 power control algorithm on each interfering user, the statistical behavior of the power-controlled fading signal of the desired user is used to model the power-controlled fading signal of each interfering user. There are two power control parameters needed to model each interfering signal: the average power $\bar{\mu}$ in equation (2.35) and its standard deviation σ_s in equation (2.36). The average power is the long-term average power of the power-controlled multipath signal of the desired user. Its standard deviation is the standard deviation of the short-term average power of the power-controlled multipath signal of the desired user. Since the received average power and its standard deviation for each interfering user are unknown, the average power and its standard deviation for each receiver are at first assumed to be reasonably guessed values and used in the simulation to model the power-controlled multipath signal of each interfering user. After many runs of simulations (i.e. at least 50 runs at 50 frames), the average power and the standard

deviation of the power-controlled multipath signal of the desired user are calculated according to equations (2.35) and (2.36). The data produced in the first frame of each run is discarded because the power control algorithm and the adaptive antenna array algorithm may not have converged yet. The recently calculated average power and its standard deviation are used to run the simulation again to obtain the new average power and its standard deviation. In the meanwhile, the BER is kept at 0.1%. If the average powers and their standard deviations produced by the subsequent simulations are very close to each other, the correctly estimated average power and its standard deviation are obtained; otherwise, the above procedure is repeated until the correctly estimated average power and its standard deviation are obtained. The correctly estimated average power and its standard deviation for each receiver, which are tabulated in Table 5.1(a) and Table 5.1(b) in Section 5.3, are used to do the following different tests.

5.2 Considerations for Phase-Dependency and Algorithm Parameters

Both phase-dependency and the values of the algorithm parameters for different adaptive antenna array algorithms are considered here. Chapter 4 shows that the performance of the recursive least squares algorithm depend on the phase of the signal, while the two modified forms of the recursive adaptive beamforming algorithm are phase-independent. This section will verify the consideration of the phase-dependency by simulation results. The values of the parameters for the selected algorithms are chosen so that the algorithms achieve the best performance in the fading channel.

The phase change for the adjacent Walsh symbols is 0.8° at a 10Hz fading rate and 8° at a 100Hz fading rate. The simulation shows that a phase change between Walsh symbols larger than about 0.3° prevents the spatial filter taps from converging under the RLS algorithm. The reason is that even minor inaccuracies in the phase estimate of the desired signal may cause major variations in the mean-square-error, $e^2(m)$, driving the algorithm (see Fig. 4.1). Hence, the RLS algorithm is truly useful for antenna array adaptation only in coherent receivers and requires a precise phase tracking mechanism at both fading rates. The simulation also shows that both RAB(a) and RAB(b) algorithms work well even with random phase changes at every Walsh symbol because both do not require the phase of the desired signal to control the taps of the spatial filters. Both are well suited to function with non-coherent receivers. In all the simulations, the phase of each path is constant for the RLS algorithm, but the phase of each path changes for both RAB algorithms.

The performance of the adaptive antenna array algorithms depends on the chosen values of the algorithms' parameters. There are two adjustable parameters in the RLS algorithm: the forgetting factor and the reference signal magnitude. When the forgetting factor is too small, the performance will depend mainly on the recent Walsh symbols. If the recent estimated Walsh symbols are inaccurate, the Walsh symbol error rate increases. Simulation shows that the RLS algorithm has a similar performance with the forgetting factor ranging from 0.999 to 0.99999 at fading rates of 10Hz and 100Hz. We have chosen the forgetting factor of 0.9999. The other parameter is the reference signal magnitude. It

must be large enough to produce the reference signals which can cancel out the desired signal component of the array output signal. Simulation shows that similar performance can be obtained when the reference signal magnitude is larger than 1.0. We have chosen a reference signal magnitude of 2 for both fading rates. There are also two adjustable parameters in the two modified forms of RAB algorithms, RAB(a) and RAB(b). The eigenvector estimation tolerance must be small enough to provide an accurate eigenvector estimation. An eigenvector estimation tolerance of 0.001 is assumed for both fading rates. Similar performance can be obtained with the forgetting factor ranging from 0.9 to 0.99. The forgetting factor is chosen to be 0.95 for both fading rates.

5.3 Power Control Parameters for Different Receivers

Power control is very important in CDMA systems. The desired signal is power-controlled by the IS-95 power control algorithm. However, for each interfering user the effect of power control is modeled as a lognormal random variable with an average power and standard deviation as in the power-controlled desired signal.

After many runs of simulations (at least 50 runs at 50 frames), the data on the instantaneous power of the desired user are collected in the presence of the interfering users which produce a 0.1% bit error rate. The average power at the input of the receiver (i.e. the total power of each interfering user) and the standard deviation for each receiver are calculated according to equations (2.35) and (2.36). These data for different receivers are tabulated in Table 5.1(a) and Table 5.1(b). The first number in each entry is the

average power $\bar{\mu}$; the second one - the standard deviation σ_s. The units are dB. Table 5.1(a) describes the 10Hz fading rate case, while Table 5.1(b) - 100Hz fading rate case. The first data column is for the 1.25MHz non-RAKE receivers; the second column - the 2.5MHz non-RAKE receivers; the third column - 1.25MHz RAKE receivers in two RAKE fingers which perfectly track the first and the third path signals; the fourth column - the 2.5MHz RAKE receivers in which the RAKE fingers receive all resolvable paths.

It is observed that the average power is lower and the standard deviation is higher at the higher fading rate for all types of receivers, except for the single-antenna and the dual-antenna non-RAKE receivers with the 1.25MHz system bandwidth. It shows that the performance of the power control algorithm deteriorates at high fading rates. The antenna array receivers governed by RLS, RAB(a) and RAB(b) have similar average powers and similar standard deviations. The antenna array receivers have higher average power than the single-antenna receivers. In the RAKE reception case, the 2.5MHz receiver has lower average power and smaller standard deviation than in the 1.25MHz case, since four RAKE fingers are used, instead of two RAKE fingers in the 1.25MHz receivers. More signal power can be extracted from the channel. In the non-RAKE reception case, the 1.25MHz antenna array receiver has lower average power and smaller standard deviation because of the assumption of the independent fading of each path and the presence of a little piece of the second path signal in the 1.25MHz system. The 1.25MHz antenna array non-RAKE receiver can exploit the second path signal from the PN-despread signal, and thus the average transmitted power is reduced. In other words,

the average power of each interfering signal is reduced. In all the simulations, the data in the Table 5.1(a) and 5.1(b) are used to model the power-controlled multipath delay profile of each interfering user.

Table 5.1(a). Power control parameters ($\bar{\mu}$, σ_s) for different receivers at 10Hz fading rate.

RAKE	no	no	yes	yes
System Bandwidth	1.25MHz	2.5MHz	1.25MHz	2.5MHz
One-Antenna	(2.86, 4.05)	(3.10, 3.85)	(1.13, 2.96)	(0.02, 2.04)
Dual-Antenna	(1.42, 3.58)	(1.59,3.36)	(0.26, 3.17)	(-0.69, 2.95)
RLS	(3.50, 3.36)	(3.87, 3.65)	(1.82, 2.59)	(0.34, 2.11)
RAB(a)	(3.41, 3.35)	(4.05, 3.67)	(1.67, 2.52)	(0.06, 2.06)
RAB(b)	(3.23, 3.22)	(3.78, 3.56)	(1.41, 2.45)	(0.02, 2.04)

Table 5.1(b). Power control parameters ($\bar{\mu}$, σ_s) for different receivers at 100Hz fading rates.

RAKE	no	no	yes	yes
System Bandwidth	1.25MHz	2.5MHz	1.25MHz	2.5MHz
One-Antenna	(1.88, 3.91)	(2.18, 4.05)	(0.69,3.66)	(-0.24, 3.54)
Dual-Antenna	(1.10, 3.78)	(1.34, 3.81)	(0.12, 3.65)	(-0.47, 3.50)
RLS	(3.39, 4.14)	(3.44, 4.18)	(1.49, 3.75)	(0.18, 3.60)
RAB(a)	(3.22, 4.19)	(3.49, 4.22)	(1.43, 3.83)	(0.03, 3.56)
RAB(b)	(2.92, 4.13)	(3.33, 4.14)	(1.34, 3.80)	(0.02, 3.53)

5.4 SINR Distribution for Different Receivers

In the thesis, the signal to interference plus noise ratio (SINR) is used to understand the performance behavior of different receivers. In the IS-95 system, the SINR of each frame can be estimated at the output of the IS-95 square-law combiner and the bit error rate of that frame can be calculated. After many runs of simulations (at least 50 runs at 50 frames), a set of data containing the SINR and the bit error rate for each frame is collected and organized to find the SINR distribution and the SINR threshold which produces 0.1% bit error rate.

Figure 5.1(a) shows the probability distribution functions for the output SINRs. The number of interfering users used in the simulation produces 0.1% BER. The solid line is a RLS non-RAKE receiver; the dashed line - a single-antenna non-RAKE receiver; the dash-dotted line - a dual-antenna non-RAKE receiver. The system bandwidth is 1.25MHz; the fading rate - 10Hz. The standard deviation of the single-antenna receiver is higher than that of the dual-antenna receiver, but narrower than that of the RLS receiver. The reason is that additional path diversity is provided for the dual-antenna receiver. In the adaptive antenna receiver, each correlated antenna array element receives the same fading signal, so the fluctuation of the received signal is much higher.

Figure 5.1(b) shows the average bit error rate for different SINRs for a single-antenna, a dual antenna and an adaptive antenna non-RAKE receiver with 1.25MHz bandwidth at 10Hz fading rate. To meet the required bit error rate of 0.1%, the required SINR thresholds for both the single-antenna and the RLS non-RAKE receivers are 11 dB; the SINR threshold for the dual-antenna receiver is 6 dB. The 5 dB gain is due to an

additional path diversity and the effect of the power control. The standard derivations of the probability distribution functions and the required SINR thresholds for different receivers at 10Hz and 100Hz fading rates are tabulated in Table 5.2(a) and 5.2(b) respectively. The first number in each entry is the SINR threshold and the second data - the standard derivation. The units are dB. It is observed that the required SINR thresholds of a single antenna and an adaptive antenna array governed by the three algorithms are similar for each type of receiver. The standard deviation of a single-antenna receiver is smaller than that of an adaptive antenna array receiver. A dual-antenna receiver has the lowest SINR threshold and the lowest standard derivation due to the additional antenna diversity. A RAKE receiver has the lowest SINR threshold and the smaller standard deviation in the resolvable path case due to the addition path diversity. A non-RAKE receiver has smaller standard deviation in the unresolvable case due to the presence of the second path. Both the required SINR threshold and the standard deviation increase with the increase in the fading rate. The reason is that the increase in fading rate will increase the fluctuation of the SINR, and thus the SINR threshold is needed to be higher to compensate the large fluctuation. Generally speaking, the adaptive antenna array receivers governed by the three algorithms exhibit similar performance. The additional path diversity improves performance, but the increased fading rate degrades it.

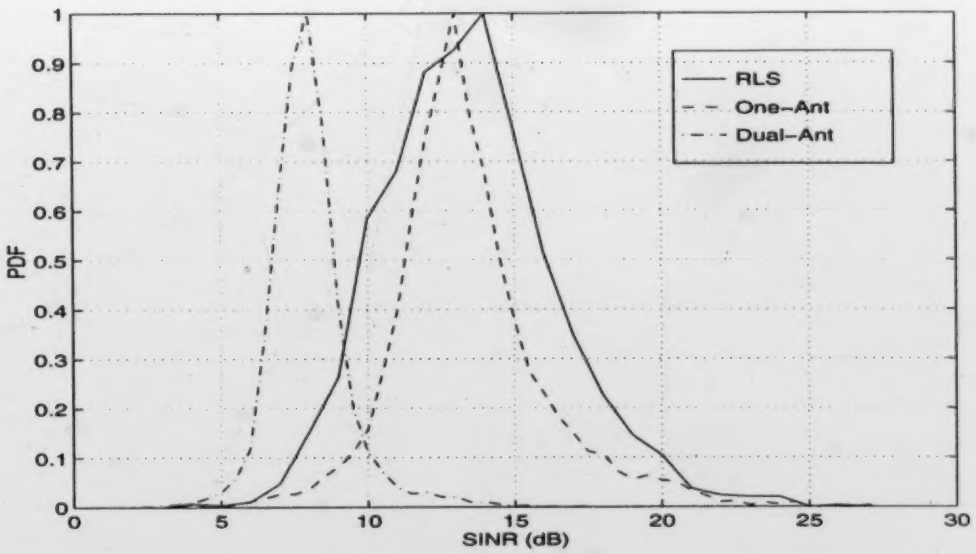

Figure 5.1(a). Probability distribution functions for the output SINRs for 0.1% BER.

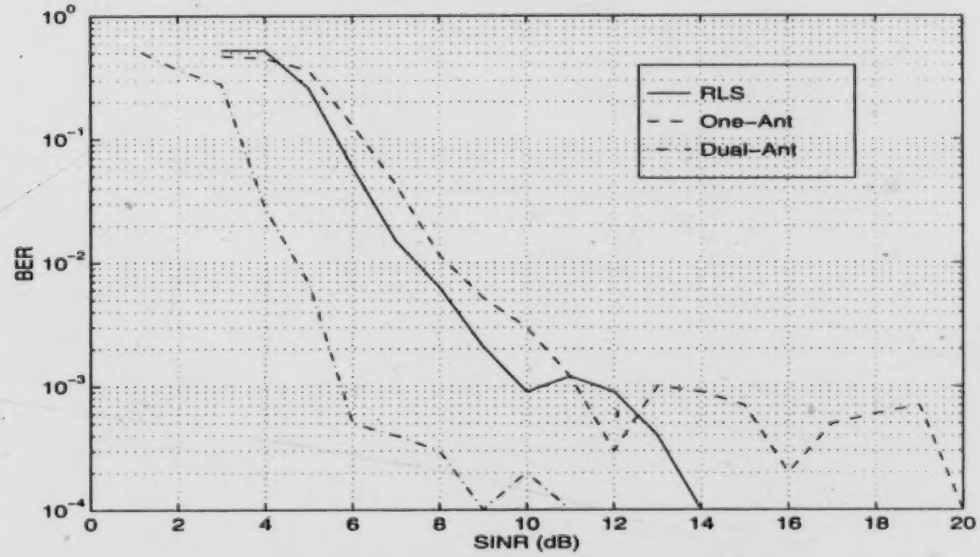

Figure 5.1(b). Average bit error rate for different SINRs.

Table 5.2(a). SINR distribution for different receivers at 10Hz fading rate.

RAKE	no	no	yes	yes
System Bandwidth	1.25MHz	2.5MHz	1.25MHz	2.5MHz
One-Antenna	(11, 2.59)	(11, 2.30)	(6.5, 1.65)	(3.5, 1.08)
Dual-Antenna	(6, 1.28)	(5.5, 1.23)	(3, 0.96)	(0.5, 0.77)
RLS	(11, 3.15)	(10, 3.69)	(6, 2.02)	(3, 1.59)
RAB(a)	(11, 2.87)	(11, 3.86)	(6, 1.89)	(4, 1.38)
RAB(b)	(11, 3.18)	(11, 3.41)	(6, 1.89)	(4, 1.49)

Table 5.2(b). SINR distribution for different receivers at 100Hz fading rate.

RAKE	no	no	yes	yes
System Bandwidth	1.25MHz	2.5MHz	1.25MHz	2.5MHz
One-Antenna	(11, 2.18)	(12, 2.26)	(8.5, 1.74)	(5.5, 1.43)
Dual-Antenna	(8, 1.49)	(7.5, 1.52)	(5, 1.27)	(2, 1.04)
RLS	(13, 3.37)	(14, 3.80)	(8, 2.21)	(5, 1.81)
RAB(a)	(13, 3.24)	(13, 3.89)	(8, 2.25)	(6, 1.69)
RAB(b)	(12, 3.34)	(11, 3.65)	(8, 2.25)	(6, 1.75)

5.5 Radiation Patterns

Radiation pattern for an antenna array with complex weights are used to observe the beamforming and nulling capabilities of an adaptive antenna array algorithm. Figure 5.2(a) shows the radiation patterns formed by the three algorithms when the number of users is 20, the fading rate - 100Hz, and the system bandwidth - 1.25MHz. The non-RAKE reception is used. Two desired signal components arrive at the base station. The solid line corresponds to RLS; the dashed line - RAB(a); the dash-dotted line - RAB(b). All three algorithms produce similar radiation patterns. They can steer their main lobes toward the first path signal at 60° and their sidelobes towards the second path signal at 145°. The second path signal has the lower signal strength. The nulls are directed at clusters of interferers. All three algorithms can successfully steer the mainlobe and second sidelobe to the desired signals and place the nulls toward the interferers.

Figure 5.2(b) shows the radiation patterns of the fourth spatial filter produced by RLS, RAB(a), and RAB(b) algorithms when the number of users is 120 (each dot represents two discrete interferers here), the system bandwidth - 2.5MHz, and the fading rate - 10Hz. The fourth spatial filter (the spatial filter operating on the fourth path in the multipath profile) has been chosen because all three algorithms can form similar radiation patterns for the first three path signals, but their performance differences are easily shown in the fourth path signal which has the lowest average power. RLS algorithm can successfully steer the main lobe towards the fourth multipath signal and create deepest nulls for the interference. The radiation pattern of RAB(b) has the lowest gain in the

mainlobe, and the highest gain for the interference. Therefore, the RAB(b) performance is expected to be the worst. It is also observed that the nulling capability is insignificant at the higher number of interferers because the spatial distribution of the interferers is more even.

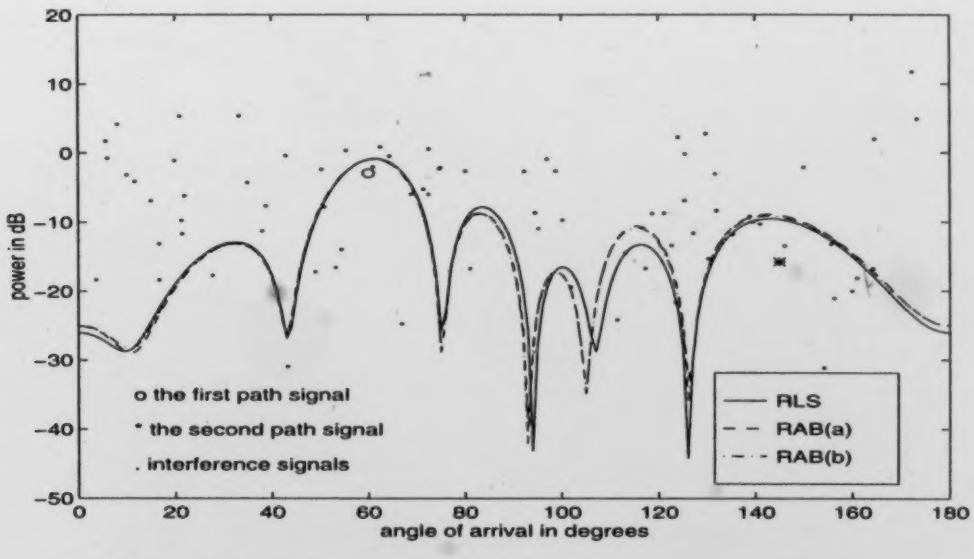

Figure 5.2(a). Radiation patterns for the unresolvable multipath case.

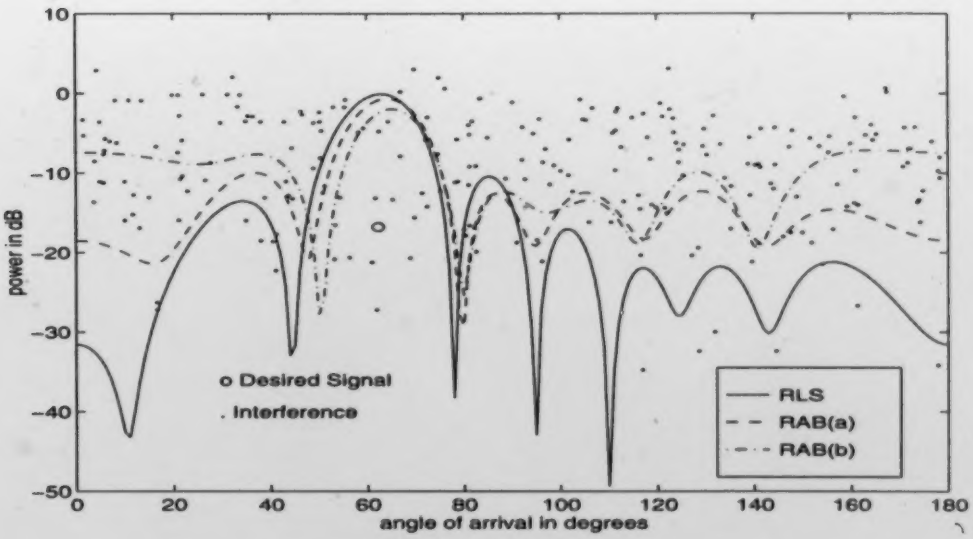

Figure 5.2(b). Radiation patterns of the fourth spatial filter.

5.6 Rates of Convergence

The system performance requirements are divided into two types: transient requirements and steady-state requirements. Transient response duration is the length of time required for the adaptive array to adjust its weights from the time it is turned on until steady-state conditions have been reached. We say that the receiver in question has reached the steady state, if the Walsh symbol error rate at its output does not exceed the maximum value acceptable for a given quality of service requirement. For single-antenna and dual-antenna receivers, in the steady state and when fading rate is relatively low, the power control algorithm eliminates most of the channel variations due to fading within the target tolerance. In the wireless fading channel, the adaptive antenna array algorithms need to converge fast enough to be able to track the fading signals of mobile users.

In the simulation, the RLS algorithm operates in a Walsh element by Walsh element manner. Since a Walsh symbol consists of 64 Walsh elements, there are 64 iterations of the algorithm during every Walsh symbol. Both RAB(a) and RAB(b) operate in a Walsh symbol by Walsh symbol manner. The desired Walsh symbol sequence is provided for the non-blind convergence test. Since for both RAB(a) and RAB(b) algorithms the error signal is not defined, we cannot compare the convergence of the three algorithms in terms of the mean-square error. Moreover, since in the fading channel we do not know the desired complex weights of the antenna array in advance, we can not compare the algorithms in terms of the difference between the converging complex weights and the ideal ones. Therefore, the convergence times for all three algorithms are compared in terms of the average Walsh symbol error rate at each elapsed Walsh symbol interval.

Since there are 64 possible transmitted Walsh symbol values, the estimated Walsh symbol values are often incorrect in the transient state, but usually correct in the steady state. During the transient interval, the channel is not yet accurately power-controlled and the radiation pattern of the array is not shaped to receive the desired signal and suppress the interferers. If we determine the Walsh symbol error rate in each individual Walsh symbol, the number of Walsh symbols required for array adaptation to generate correct estimated Walsh symbols can be found (i.e. within the target symbol error rate). Figure 5.3 shows the results for the rates of convergence for different 2.5MHz non-RAKE receivers at a 10Hz fading rate. The number of simulation runs for each receiver is 1000. The simulated interfering users produce decoded 0.1% BER in the steady state (i.e. 3

interfering users are simulated in the single-antenna receiver; 16 users - in the other receivers). The Walsh symbol error rate of the first Walsh symbol for RLS algorithm is 0.45%; for RAB(a) and RAB(b) algorithms they are 0.32%. The ensemble-averaged learning curve of the RLS algorithm is higher than for both RAB algorithms, so the RAB algorithms converge faster. The RAB(a) algorithm performs the best. The learning curves of the single-antenna and the dual-antenna receivers are quite flat and converge gradually, and the symbol error rate at the first Walsh symbol is only 0.1%. The region ranging from the 10-th to the 30-th Walsh symbols for the adaptive antenna array receivers declines gradually because the power control algorithm has not eliminated the variations of the channel fading within the target tolerance. In the steady state of the 1.25MHz non-RAKE systems at 10Hz fading rate, the average Walsh symbol error rate for the single-antenna receiver is 2.0%; for the dual-antenna receiver - 2.6%; for the adaptive antenna array receivers - 1.2%. At 100Hz fading rate, the average Walsh symbol error rates for the single-antenna and dual-antenna receivers are 7%; for the adaptive antenna array receivers - 5%. The Walsh symbol error rates in the steady state increases at higher fading rates because the target decoded bit error rate is 0.1% for all receivers and the coding gain, due to the 64-ary Walsh demodulation, the 1/3 convolutional decoder, and bit-by-bit de-interleaver, is higher at the higher fading rate. In conclusion, the 2.5MHz non-RAKE adaptive antenna array receivers require about 10 Walsh symbols to successfully shape the radiation patterns when the desired Walsh symbols are provided for convergence.

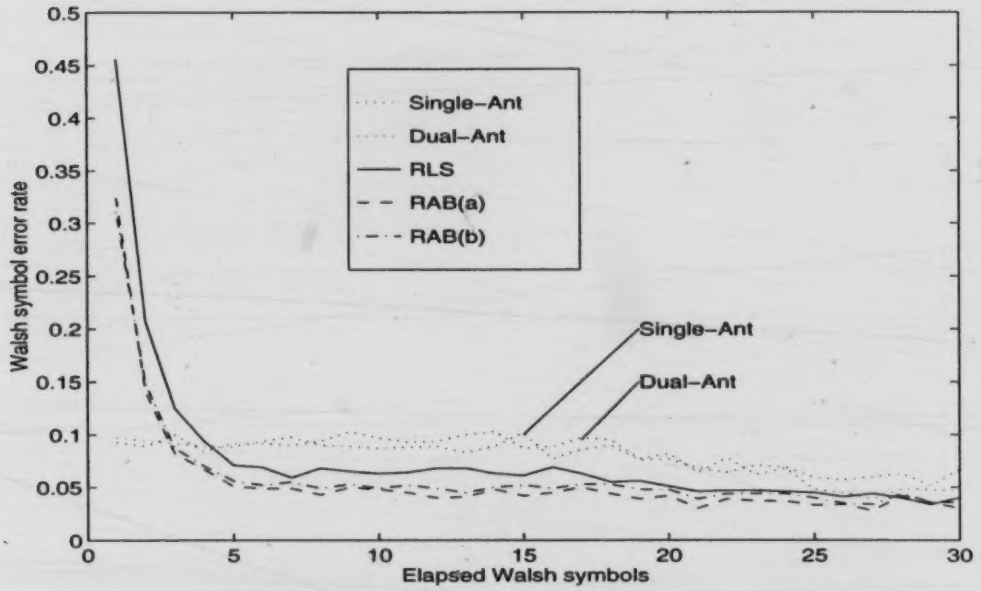

Figure 5.3. Rates of convergence for different 2.5MHz non-RAKE receivers at 10Hz fading rate.

5.7 User Capacity for Different Receivers

User capacity is the number of users that can be accommodated in the system at a given level of quality of service. To simplify the simulation of the 2.5MHz system, only half of all interfering power-controlled and faded other user signals are simulated, but their average powers are increased by a factor of two in comparison with 1.25MHz simulation. This approach causes some underestimation of the capacity of the 2.5MHz system. The user capacity, discussed in this section, does not include the effect of intermittent voice activity, which in principle should double the capacity numbers. On the other hand, the effect of the inter-cell interference (not included in the analysis) is opposite and of approximately the same magnitude as that of intermittent voice activity. Hence, capacity

results for a single-cell system which does not take advantage of voice activity can be used as first approximation of those for a multi-cell system with voice-activity control of transmissions.

Figures 5.4(a) and 5.4(b) show the user capacity curves per 1.25MHz system bandwidth for different types of receivers without RAKE combining at fading rates of 10Hz and 100Hz respectively. The solid line denotes the capacity produced by the 2.5MHz system in the fully resolvable path scenario, while the dotted line is for the 1.25MHz system (unresolvable path scenario). The 1.25MHz and the 2.5MHz systems exhibit similar performance in both the single-antenna and the dual-antenna reception cases at both fading rates. However, the 1.25MHz system outperforms the 2.5MHz system in the adaptive antenna array reception case, because the adaptive antenna array is able to shape its radiation pattern to receive desired signals arriving on both the first and the second paths in 1.25MHz system.

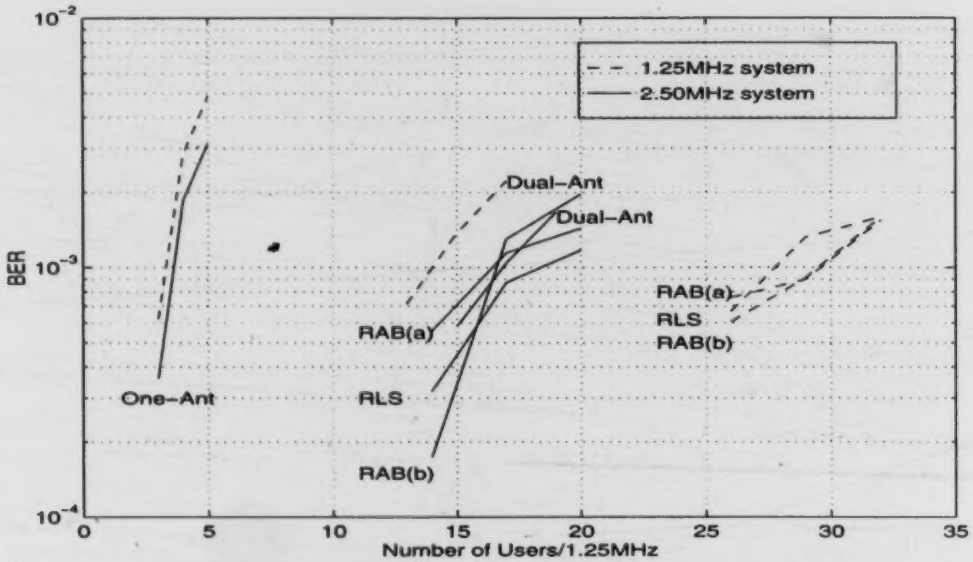

Figure 5.4(a). User capacity for different non-RAKE receivers at 10Hz fading rate.

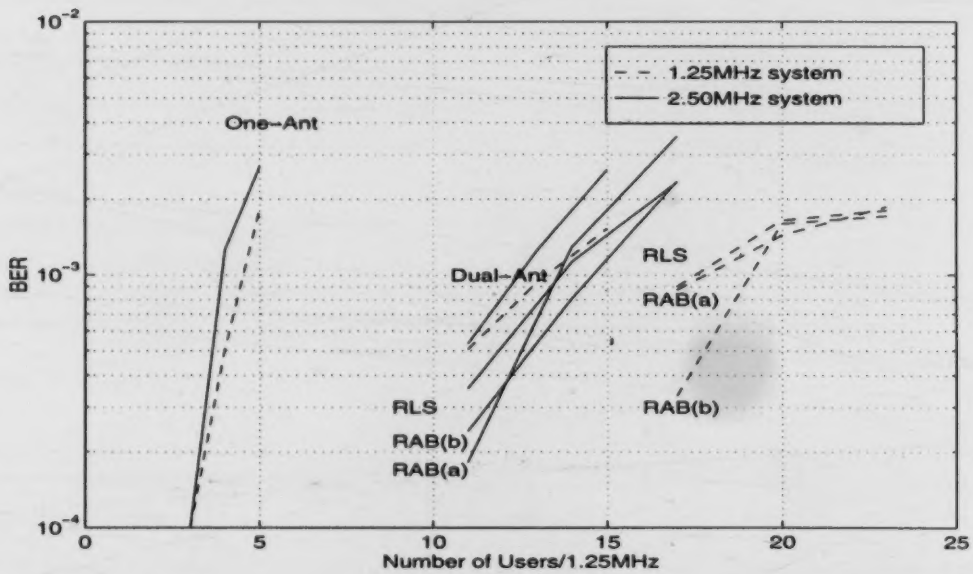

Figure 5.4(b). User capacity for different non-RAKE receivers at 100 Hz fading rate.

Figures 5.4(c) and 5.4(d) show the user capacity per 1.25MHz system bandwidth for different RAKE receivers at fading rates of 10Hz and 100Hz, respectively. The 2.5MHz system outperforms the 1.25MHz system for all types of RAKE receivers because four spatial filters are used in the resolvable multipath case, instead of two in the unresolvable one.

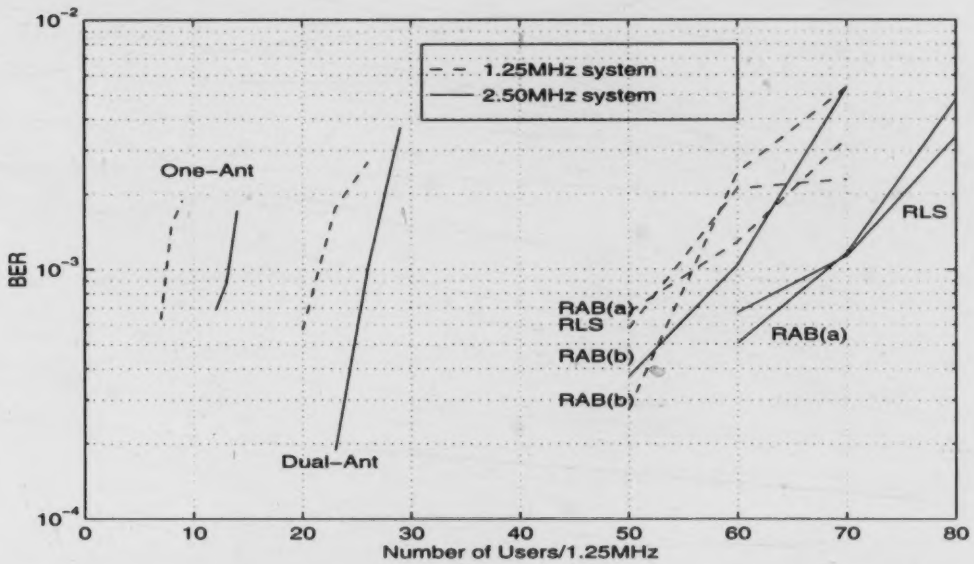

Figure 5.4(c). User capacity for different RAKE receivers at 10Hz fading rate.

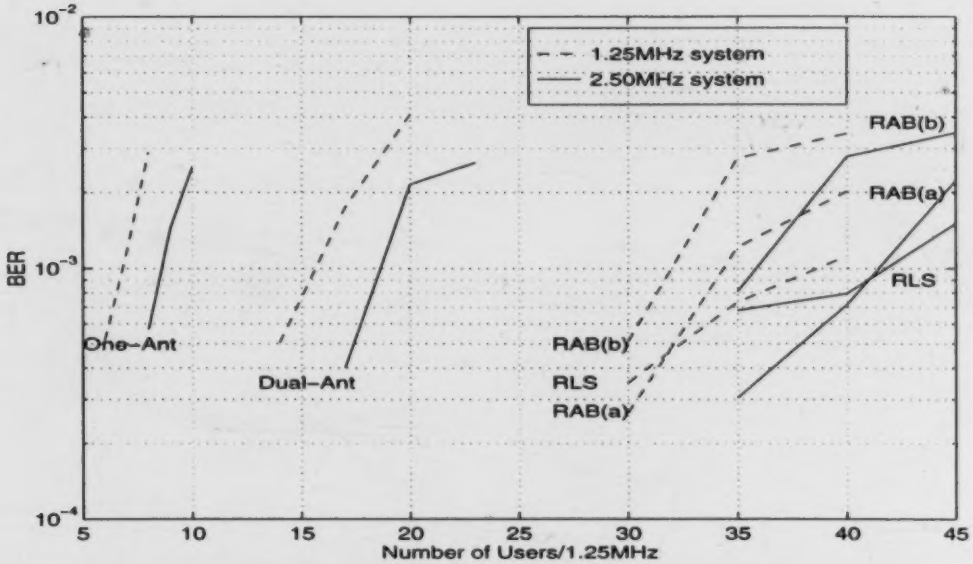

Figure 5.4(d). User capacity for different RAKE receivers at 100Hz fading rate.

Figure 5.4(e) shows the user capacity for different types of RAKE receivers in the 1.25MHz system at fading rates of 10Hz and 100Hz. For each type of receiver, performance degrades with an increase in fading rate.

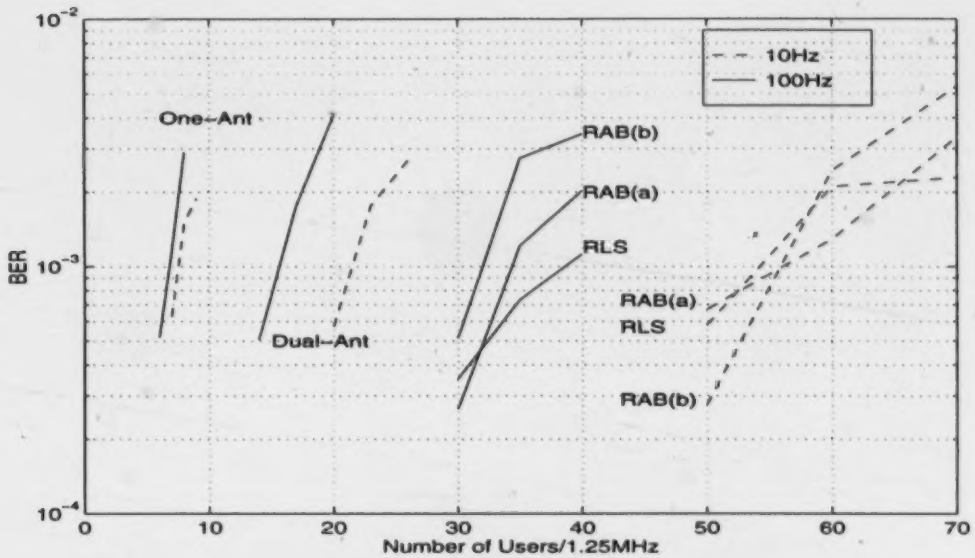

Figure 5.4(e). User capacity for different fading rates.

Tables 5.3(a) and 5.3(b) show the user capacity per 1.25MHz bandwidth at the bit error rate of 0.1% for different types of receivers at fading rates of 10Hz and 100Hz, respectively. The current IS-95 receiver is the 1.25MHz dual-antenna RAKE receiver. Let's Consider the worst case situation at 100Hz fading rate and with the use of RAB(b) algorithm. The user capacity of the dual-antenna RAKE receiver is 16; the capacity of the RAB(b) RAKE receiver is 32. The adaptive antenna array RAKE receiver containing eight antenna elements at least doubles the user capacity of the current dual-antenna RAKE receiver.

Table 5.3(a). User capacity for different receivers at 10Hz fading rate.

RAKE	no	no	yes	yes
System Bandwidth	1.25MHz	2.5MHz	1.25MHz	2.5MHz
One-Antenna	4	4	7	13
Dual-Antenna	14	16.5	21	26
RLS	27.5	18	55	68
RAB(a)	29.5	16.5	56	68
RAB(b)	29.5	16.5	56	60

Table 5.3(b). User capacity for different receivers at 100Hz fading rate.

RAKE	no	no	yes	yes
System Bandwidth	1.25MHz	2.5MHz	1.25MHz	2.5MHz
One-Antenna	4.5	4	7	8.5
Dual-Antenna	13	12.5	16	18.5
RLS	18	13.5	38.5	42
RAB(a)	18	13.5	34	41.5
RAB(b)	19	14.5	32	36

5.8 Summary

This chapter has shown that adaptive antenna array receivers governed by the recursive least square algorithm and the two modified forms of the recursive adaptive beamforming algorithm can successfully steer the main lobe towards the desired signal, and place the nulls towards the interference. Thus, the multiple access interference is significantly reduced and the user capacity is improved. The recursive least squares algorithm slightly outperforms the two modified forms of the recursive adaptive beamforming, but it requires a phase tracking mechanism. The two modified forms of the recursive adaptive beamforming exhibit faster convergence than the recursive least squares algorithm. The adaptive antenna non-RAKE receiver extracts more energy than other non-RAKE receivers in the unresolvable path case. The performance degrades with an increase in fading rate. The eight-element adaptive antenna RAKE receiver achieves at least double the user capacity of the current IS-95 dual-antenna RAKE receiver.

6. CONCLUSION

The main focus of this thesis has been the implementation of advanced adaptive antenna array reception techniques on the reverse link of the IS-95 CDMA system. Narrowband and wideband systems have been considered at fading rates of 10Hz and 100Hz with non-coherent multipath combining. This work has been prompted by the current thrust in wireless communication technology to support the future capacity demands with the introduction of new personal communication services.

6.1 Thesis Summary

In this work, the three chosen algorithms, the recursive least squares algorithm and two modified forms of recursive adaptive beamforming, are compared on the reverse link of an IS-95 CDMA system. Chapter 2 presented the channel and the system models of the IS-95 system in the microcellular environment. The statistical models for a scalar (single antenna) channel and a vector (antenna array) channel have been presented. The simplified models of the transmitter as well as a single-antenna, a dual-antenna, and an antenna array receivers have been presented. The power control algorithm has also been described.

In Chapter 3, the working idea of the adaptive antenna array has been illustrated using a simple beamformer. The effect of the array geometry and structure have been explained. The different antenna array adaptation techniques have been reviewed, such as a switched beam system, a simple beamformer, subspace-based techniques, eigenfilter

techniques, and optimum combining techniques. The latter exhibits the best performance. In Chapter 4, the optimum combining techniques are implemented in the IS-95 CDMA reverse link. Detailed derivations of the recursive least squares algorithm and two modified forms of recursive adaptive beamforming have been presented.

The simulation results of all three algorithms have been presented in Chapter 5. All three algorithms can successfully enhance the desired signal by steering the main lobe and suppress the interference by placing nulls. The recursive least squares algorithm slightly outperforms the two modified forms of recursive adaptive beamforming, but it requires a precise phase tracking mechanism. The recursive least squares algorithm also requires a longer convergence time than the two modified forms of recursive adaptive beamfoming algorithms. The adaptive antenna array receiver extracts more energy than omni-directional antenna receivers in the unresolvable path case. The eight-element adaptive antenna array RAKE receiver achieves at least double the user capacity of the current IS-95 dual-antenna RAKE receiver.

6.2 Future Directions

Although this thesis has implemented the adaptive antenna array in the IS-95 CDMA system and shown the capacity improvement over the current IS-95 system, further investigation including the following is desirable:

- Multi-user detection can be implemented with adaptive antenna array techniques to eliminate any strong interference arriving within the mainlobe and sidelobes.
- The base station must be also able to use beamforming on the forward link to effectively improve overall system performance. However, since both forward and reverse links use different frequency bands for transmission, the multipath propagation channels for both links are quite different.
- The chosen channel is typical of the urban microcellular environment. Different channel environments should be investigated for the future third-generation mobile communications systems.

REFERENCES

[1] Theodore S. Rappaport, *Wireless Communications*, Prentice Hall, Upper Saddle River, New Jersey, 1996, pp. 1-3, 169, 325-338.

[2] Jay E. Padgett, Christoph G G. Gunther, and Takeshi Hattori, "Overview of wireless personal communications", *IEEE Commun. Mag.*, vol. 33, no. 1, Jan. 1995, pp. 28-41.

[3] Ramjee Prasad, "Overview of wireless personal communications: microwave perspectives", *IEEE Commun. Mag.*, vol. 35, no. 4, Apr. 1997, pp. 104-108.

[4] Ryuji Kohn, Reuven Meidan, and Laurence B. Milstein, "Spread Spectrum Access Methods for Wireless Communications," *IEEE Commun. Mag.*, vol. 33, no. 1, January, 1995, pp. 58-67.

[5] TIA/EIA IS-95, "Mobile station - base station compatibility standard for dual-mode wideband spread spectrum cellular system", Telecommunications Industry Association, 1993.

[6] Ayman D. Naguib, and Arogyaswami Paulraj, "Capacity improvement with base-station antenna arrays in cellular CDMA," *IEEE Transactions on Vehicular Technology*, vol. 43, no. 3, Aug. 1994, pp. 691-698.

[7] Joseph C. Liberti, Jr. and Theodore S. Rappaport, "Analytical results for capacity improvements in CDMA", *IEEE Transactions on Vehicular Technology*, vol. 43, no. 3, August 1994, pp. 680-690.

[8] John S. Thompson, Peter M. Grant, and Bernard Mulgrew, "Smart Antenna Arrays for CDMA Systems", *Personal Communication*, vol. 3, no. 5, October 1996, pp. 16-25.

[9] John S. Thompson, Peter M. Grant and Bernard Mulgrew, "Performance of Antenna Array Receiver Algorithms for CDMA", *1996 IEEE Global Telecomm. Conf.*, November pp. 570-574.

[10] David P. Whipple, "CDMA Standard", *Applied Microwave & Wireless*, Winter, 1994, pp. 24-39.

[11] Jorgen Bach Andersen, Theodore S. Rappaport, and Susumu Yoshida, "Propagation Measurements and Models for Wireless Communications Channels", *IEEE Commun. Mag.*, vol. 33, no. 1, January, 1995, pp. 42-49.

[12] Li Fung Change, Fuyun Ling, David D. Falconer, and Nelson R. Sollenberger, "Comparison of two convolutional orthogonal coding techniques for CDMA radio communications systems", *IEEE Trans. on Commun.*, vol. 43, no. 6, June 1995. pp. 2028-2037.

[13] Alexandra Duel-Hallen, Jack Holtzman, and Zoran Zvonar, "Multiuser detection for CDMA systems", *IEEE Personal Communication*, vol. 2, no. 2, April, 1995, pp. 46-58.

[14] Shimon Moshavi, "Multi-user detection for DS-CDMA communications", *IEEE Commun. Mag.*, vol. 34, no. 10, October, 1996, pp. 124-136.

[15] Asha Metrotra, *Cellular Radio Performance Engineering*, Artech House Inc., Norwood, MA, 1994, pp. 349-362.

[16] Gordon L. Situber, *Principle of Mobile Communication*, Kluwer Academic Publishers, Norwell, Massachusetts, 1996, pp. 250.

[17] G.V. Tsoulos, M.A. Beach. S.C. Swales, "Adaptive antennas for third generation DS-CDMA cellular systems", *Proc. VTC'95*, Chicago, USA, July 1995, pp. 45-49.

[18] A.F. Naguib, A. Paulraj, "Recursive adaptive beamforming for DS-CDMA", *Proc. ICC'95*, Seattle, USA, June 1995, pp.1515-1519.

[19] JTC(AIR)-238R2, "Final report on RF channel characterization", *Joint Technical Committee on Wireless Access*, December 1993.

[20] S. Unnikishna Pilai, *Array Signal Processing*, Springer-Verlag New Yourk Inc., 189, pp. 6-7, 10-18, 28-33.

[21] A. Jalali and P. Mermelstein, "Effects of ,Diversity, Power Control and Bandwidth on the Capacity of Microcellular CDMA systems", *IEEE J. Select. Areas. Commun.*, vol. JSAC-12(5), June 1994.

[22] S. Ariyavisitakul and L. F. Chang, "Signal and Interference Statistics of a CDMA System with Feedback Power Control", *IEEE Trans. Commun.*, vol. 41, no. 11, November 1993, pp. 1626-1634.

[23] Ryuji Konhno, Predag B. Rapajic, and Branka S. Bucetic, "An overview of adaptive techniques for interference minimization in CDMA system", *Wireless Personal Communications*, vol. 1, no. 1, January, 1994, pp. 3-21.

[24] Robert A. Monzingo & Thomas W. Miller, *Introduction to Adaptive Arrays*, John Wiley & Sons, Inc., pp. 9, 34-47, 429-433.

[25] Joseph C. Liberti and Theodore S. Rappaport, "Analysis of CDMA cellular radio systems employing adaptive antennas in multipath environments", *VTC'96*, pp. 1076-1080.

[26] Manouchehr Mahmoudi and Elvino S. Sousa, "Sectorized antenna system for CDMA cellular networks", *VTC'97*, vol. 1, pp. 6-9.

[27] Yiping Wang and J. R. Cruz, "Augmented antenna arrays for CDMA cellular systems", *VTC'96*, pp. 1091-1095.

[28] Yiping Wang and J. R. Cruz, "Performance analysis of CDMA cellular systems with adaptive antenna arrays over multipath channels", *VTC'96*, pp. 536-540.

[29] Jian-Guo Wang and Ananda S. Mohan, "An adaptive antenna array with parallel beamformers for indoor radio channel enhancement", *VTC'97*, pp. 188-192.

[30] Gene H. Golub, Charles F. Van Loan, *Matrix Computations*, The Johns Hopkins University Press, 1983, pp. 209-211.

[31] D. K. Faddeev and V. N. Faddeeva, *Computational Methods of Linear Algebra*, W.H.Freeman and Company, 1963, pp. 291-295.

[32] Bernard D. Steinberg, *Principles of Aperture and Array System Design*, John Wiley & Sons, Inc., 1976, pp. 262-265.

[33] Simon Haykin, *Adaptive Filter Theory*, Prentice-Hall, Inc., New Jersey, 1991, pp. 477-486.

[34] Michel C. Jeruchim, Philip Balaban and K., Sam Shanmugan, *Simulation of Communication Systems*, Plemum Press, New York, 1992, pp. 463-550.